A COMPARATIVE STUDY OF DIELECTRIC MATERIALS AND METALS AS NANOPLASMONIC WAVEGUIDES

By:

FERDOUS S. AZAD
MD. SAHABUL HOSSAIN
MOHAMMED TANVIR AHMED

BACHELOR OF SCIENCE
IN
ELECTRICAL AND ELECTRONIC ENGINEERING

ISLAMIC UNIVERSITY OF TECHNOLOGY (IUT)
A Subsidiary Organ of Organization of Islamic Cooperation (OIC)
Dhaka, Bangladesh.
November, 2015

ISLAMIC UNIVERSITY OF TECHNOLOGY (IUT)

A COMPARATIVE STUDY OF DIELECTRIC MATERIALS AND METALS AS NANOPLASMONIC WAVEGUIDES

By:
Ferdous S. Azad (112442)
Md. Sahabul Hossain (112405)
Mohammed Tanvir Ahmed (112406)

Supervised by:
Rakibul Hasan Sagor
Assistant Professor,
Department of Electrical and Electronic Engineering,
Islamic University of Technology.

Declaration of Authorship

We, Ferdous S. Azad (112442), Md. Sahabul Hossain (112405) and Mohammed Tanvir Ahmed (112406), declare that this thesis titled 'A comparative study of dielectric materials and metals as nanoplasmonic waveguides' has been done for the partial fulfillment of the degree of Bachelor of Science in Electrical and Electronic Engineering at Islamic University of Technology. Where we have consulted the published work of others, we have always clearly attributed the sources.

Submitted by:

Ferdous S. Azad (112442)

Md. Sahabul Hossain (112405)

Mohammed Tanvir Ahmed (112406)

A COMPARATIVE STUDY OF DIELECTRIC MATERIALS AND METALS AS NANOPLASMONIC WAVEGUIDES

Approved By:

Rakibul Hasan Sagor
Thesis Supervisor,
Assistant Professor,
Department of Electrical and Electronic Engineering,
Islamic University of Technology.

Prof. Dr. Md. Shahid Ullah
Head of the Department,
Department of Electrical and Electronic Engineering,
Islamic University of Technology.

Acknowledgement

First and foremost, we offer deepest gratitude to the Almighty Allah (SWT) for giving us the capability to do this work with good health.

We are grateful to our research supervisor, Rakibul Hasan Sagor, for the support and guidance throughout our research at Islamic University of Technology (IUT) since August 2014. He created a research environment for which we were able to explore many ideas without constraint. We have gained a wealth of knowledge and experience in science and engineering through his direction that is beyond value to our future endeavor.

We would like to thank all the faculty members of the department of EEE, IUT for their inspiration and support.

We are also thankful to our family, friends and well-wishers for their support and inspiration. Without them it would never have been possible for us to make it this far.

Abstract

The ability of Surface Plasmon Polaritons (SPPs) to overcome the diffraction limit has made it a field of great research interest. It is being predicted that next generation microchips will be produced using plasmonics-electronics hybrid technology. This will solve the RC delay issue of current electronic microchips and scaling issue of conventional integrated photonic devices. However, there are some shortcomings of SPP which are higher losses in the metallic layer and less propagation distance. Using current technology, propagation distance of SPP cannot exceed the benchmark of micrometers. The objective of this thesis is study the power transmission characteristics of different kinds of waveguides for several materials and analyze their performance using the FDTD method. SPP propagation characteristics through different optical nanostructures having different geometries have been investigated to analyze the performance of the materials. Waveguides with different kinds of bends have been investigated and compared with each other to see the effects of these bends on the efficiency of power transmission. All of the simulations have been done for a range of signal wavelength extending beyond the visible light spectrum.

Contents

List of figures

Abbreviations

ABC	Absorbing Boundary Condition
ADE	Auxiliary Differential Equation
AlAs	Aluminum Arsenide
DMD	Dielectric-Metal-Dielectric
FDTD	Finite Difference Time Domain
GLS	Gallium Lanthanum Sulfide
IR	Infra-Red
LD	Lorentz-Drude
MDM	Metal-Dielectric-Metal
PLRC	Piecewise Linear Recursive Convolution
PML	Perfectly Matched Layer
SPP	Surface Plasmon Polariton
TE	Transverse Electric
TM	Transverse Magnetic

Chapter 1

Introduction and Background

1.1 Introduction

The interaction between light and matter being a subject of study for hundreds of years has become an interest of research in recent times. Since the inception of modern science, research on light had been extended to beyond the visible spectra (400nm to 750 nm) [1]. Exploring the interaction between light and matter has enabled us to explore a vast variety of natural phenomena, from the nanoparticle interactions to the birth of giant stars. Now it is possible to exploit light matter interaction at nanoscale due to recent advances in fabrication technology.

With shrinkage of device size, the classical electronic devices face problems like heat dissipation and slower speed. Many demerits and constraints of existing technologies can be overcome using light as the information carrier. Classically, fundamental limit of using light is set by the wavelength of light. Any type of propagating waves cannot be focused to smaller dimension than half of wavelength[2]. This limit of wavelength is diffraction limit. The optical chips will not require any insulation since photons do not interact with each other, making the system lighter[3] [4]. As Plasmonics has the ability to overcome the diffraction limit, it has attractive research areas [5-7]. The diffraction limit can be overcome by making the use of 'light-matter interaction' at metal surface [5] [7].

A plasmon is a quasiparticle which arises from the quantization of plasma oscillations. Plasmons can couple with a photon to create another quasiparticle called a plasmon polariton. Surface plasmons (SPs) are coherent delocalized electron oscillations that exist at the interface between any two materials. Surface plasmon polaritons (SPPs), are infrared or visible-frequency electromagnetic waves, which travel along a metal-dielectric or metal-air interface. SPP can overcome diffraction limit which has widened the area of new applications[8] [9].

Plasmonic devices work as bridge between optical devices and sub-wavelength electronics devices. Plasmonic devices can operate very fast. On the other hand, it minimizes the size of integrated devices. Limitation of plasmonic devices is the decay rate of plasmons which is very fast [6].

The computation power of computer chips will increase drastically if plasmonic based integrated circuits can be designed. Functional plasmonic nanocircuits are already demonstrated experimentally [10] .

Researchers have achieved enormous improvement of performance and higher efficiency in solar cell technology using plasmonics. The problems of silicon based solar cells can be solved by this technology. Metal nanoparticles can be used on the surface of thin film silicon cells[11]. Plasmon enhanced solar cells has increased the absorption efficiency significantly [12] [13] [14].

The other applications of plasmonics are biosensing [15] , sub-wavelength imaging [16] [17] [18], metamaterials [19] and Bragg's reflector [20].

1.2 Overview of Surface-Plasmon-Polariton

Surface plasmon polaritons are electromagnetic excitations propagating at the interface between a dielectric and a conductor, evanescently confined in the perpendicular direction [6]. When a metal is exposed to light in a certain way, the incident light excites the electrons on the surface of the metal which causes electron oscillation. Plasmon, the unit of plasma oscillation, can be excited inside the metal by incident light outside the metal. When plasmons and photon are coupled together, the resulting hybridized excitation is known as Surface Plasmon-Polariton (SPP).

The surface excitations can be characterized in terms of their dispersion and spatial profile. The SPPs propagation along the surface of a metal continues until the energy is lost by absorption in the metal or by radiation. Considering a flat interface between a dielectric and metal having dielectric constants ε_d and ε_m and respectively, SPPs are TM plane wave solution of Maxwell's equations which propagate along the metal-dielectric interface. Therefore, SPPs exist only in the vicinity of the interface that results in a nanoscale confinement of the optical waves. If the interface is normal to z axis and the propagation direction of SPPs is along the x direction, the SPP wave vector k_x can be related to the optical frequency through the dispersion relation [21].

$$k_x = k_0\sqrt{\frac{\varepsilon_d\varepsilon_m}{\varepsilon_d+\varepsilon_m}} \tag{1.1}$$

Where, $k_0=\frac{\omega}{c}$ is the free-space wave vector. We take ω to be real and allow k_x to be complex, since our main interest is in stationary monochromatic SPP fields in a finite area [22]. The details of SPP have been discussed in **Chapter 2**.

1.3 Literature Review

The research in plasmonics started as early as 1950. But it has gained considerable acceleration in recent years. Surface-Plasmon-Polariton (SPP) has been a field of great research interest for the past few years. Several research works have been done on this topic. Researchers are also working on Material modeling. Our main focus of the literature review will be on the published works that are related to material modeling parameter extraction and SPP propagation analysis through different structures.

The parameters of several metals have been known through published works in this field. Jin et al. [23] determined the modified Debye model parameters for gold which are applicable in the wavelength range of 550-950 nm. Krug et al. [24] reported the gold parameters that are applicable in the wavelength range of 700-1000 nm. W.H.P. Pernice et al. [25] extracted the parameters for Nickel using Lorentz-Drude model. A.D. Rakic et al. [26] reported the parameters for Nickel, Palladium, Titanium and 8 other metals using Lorentz-Drude and Brendel-Bormann Model. M.A. Ordal et al. [27] extracted the parameters for fourteen metals in the infrared and far-infrared range.

The propagation loss of SPP is very high in MDM configuration of plasmonic waveguide that limits propagation length. Even the fabrication related disorders have far less impact on the propagation loss than the losses that occur in metallic layers of the Metal Dielectric Metal waveguide. This problem can be addressed by using both plasmonic and dielectric waveguide on the same chip [28]. The dielectric waveguide will carry the fundamental optical mode and the plasmonic waveguide will address the sub-wavelength scale issue. For this reason, efficient coupling of optical modes from the dielectric waveguide to the plasmonic waveguide is necessary. Therefore, designing efficient nanoplasmonic couplers with different materials and structures can be a stepping step in miniaturization of the integrated photonic devices. In the recent past, several plasmonic couplers have been proposed by different researchers. G. Veronis et. al. [29] proposed a coupler with multi-section tapers. P. Ginzburg et al. [30] reported a one-fourth of wavelength coupler to couple optical modes from a

0.5m to 50nm wide plasmonic waveguide. R. Washleh et al. [31] reported an analysis on nanoplasmonic air-slot coupler and its fabrication steps.

1.4 Thesis Organization

The thesis has been arranged in the following way-

- In **Chapter 2**, the basic theory of SPP propagation has been described. This chapter introduces the fundamental knowledge and necessary mathematical formulations of SPP propagation at the single and double interface.
- In **Chapter 3**, the widely used models for modeling metals have been described in detail with necessary derivations. Since SPPs are created due to the coupling of photon energy to the free electrons of metal, modeling metals is one of the key steps for the simulation of SPP propagation.
- **Chapter 4** introduces the fundamentals of the FDTD algorithm for 1D and 2D simulations. The original formulations of Yee do not include the frequency dependent dispersion properties of materials. We have used the ADE based general algorithm for our simulation model which is discussed in Chapter 4. This chapter also discusses about the absorbing boundary condition.
- **Chapter 5** discusses the analysis of SPP propagations through various nanoplasmonic waveguides. The waveguides are simulated for different signal frequencies and different materials. Three types of waveguides are simulated for transmission efficiency calculation. The first one is a simple straight waveguide, the second one is with a 90° sharp bend and the last one is with a circular bend. The results are compared with each other to see the effects of these bends.
- In **Chapter 6**, we have provided the summary and discussed about future plans.

Chapter 2

SPP Propagation Theory

2.1 Introduction

Surface Plasmon polariton is a quasiparticle, which propagates like an electromagnetic wave along the interface between two materials, metal and dielectric medium. The wave undergoes exponential decay as it propagates into the material from the metal-dielectric interface. The wave electromagnetic wave propagation is obtained from the solution of Maxwell's equation into each medium. Maxwell's equations of macroscopic electromagnetism can be written as follows:

From Gauss's law for the electric field:

$$\nabla . D = \rho_{ext} \tag{2.1}$$

From Gauss's law, for the magnetic field:

$$\nabla . B = 0 \tag{2.2}$$

From Faraday's Law:

$$\nabla \times \mathrm{E} = -\frac{\partial \mathrm{B}}{\partial \mathrm{t}} \tag{2.3}$$

From Ampere's Law:

$$\nabla \times \mathrm{H} = \mathrm{J_{ext}} + \frac{\partial \mathrm{D}}{\partial \mathrm{t}} \tag{2.4}$$

Here,

E is the electric field vector (V/m)
D is the electric flux density vector (C/m^2)
H is the magnetic field vector (A/m)
B is the magnetic flux density vector (Wb/m^2)

ρ_{ext} is the charge density

J_{ext} is the current density

The four macroscopic fields can be also linked further via the polarization (P) and magnetization (M) by:

$$D = \varepsilon_0 E + P \tag{2.5}$$

$$H = \frac{1}{\mu_0} B - M \tag{2.6}$$

Simplifying these equations for linear, isotropic and nonmagnetic media as:

$$D = \varepsilon_0 \varepsilon_r E \tag{2.7}$$

$$B = \mu_0 \mu_r H \tag{2.8}$$

where,

ε_0 is electric permittivity of vacuum (F/m)

μ_0 is the magnetic permeability of vacuum (H/m)

ε_r is the relative permittivity

μ_r is the relative permeability

2.2 Electromagnetic Wave Equation:

Deriving from Maxwell's equation we can obtain the field amplitude in time and space of the EM wave equation. This is done by taking curl of Faraday's law.

$$\nabla \times \nabla \times E = -\frac{\partial B}{\partial t} \tag{2.9}$$

or,

$$\nabla \times \nabla \times E = \nabla \times \left(-\mu \frac{\partial H}{\partial t}\right) \tag{2.10}$$

Using the identities $\nabla \times \nabla \times E = \nabla(\nabla.E) - \nabla^2 E$ and $\nabla \times H = \varepsilon \frac{\partial E}{\partial t}$, we can simplify the above equation as

$$\nabla(\nabla.E) - \nabla^2 E = -\mu\varepsilon\frac{\partial^2 E}{\partial t^2} \quad (2.11)$$

From Gauss's law we can conclude that the divergence of electric field E in a constant permittivity over space is zero. i,e $\nabla.E = 0$.

Therefore, the final wave equation will be (for electric field):

$$\nabla^2 E - \mu\varepsilon\frac{\partial^2 E}{\partial t^2} = 0 \quad (2.12)$$

The wave equation of magnetic field is derived as

$$\nabla^2 H - \mu\varepsilon\frac{\partial^2 H}{\partial t^2} = 0 \quad (2.13)$$

Therefore, the general form of wave equation is written as:

$$\nabla^2 U - \frac{1}{\upsilon_p^2}\left(\frac{\partial^2 H}{\partial t^2}\right) = 0 \quad (2.14)$$

If the variation of the dielectric profile ε is negligible over distance, then we can write:

$$\nabla^2 E - \frac{\varepsilon}{c^2}\left(\frac{\partial^2 E}{\partial t^2}\right) = 0 \quad (2.15)$$

Where $c = \frac{1}{\sqrt{\varepsilon_0\mu_0}}$, velocity of light.

The solution of wave equation is a harmonic function in time and space. Now assuming as a harmonic time dependence of the electric field,

$$E(r, t) = E(r)e^{-jt\omega} \quad (2.16)$$

So, the Helmholtz equation is:

$$\nabla^2 E + k_0^2\varepsilon E = 0 \quad (2.17)$$

Where the vector of propagation $k_0 = \frac{\omega}{c}$

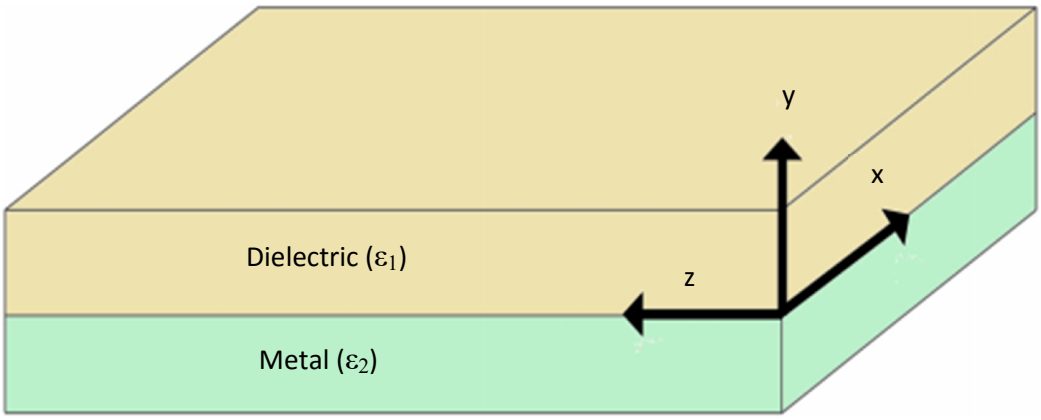

Fig 2.1: Typical planar waveguide geometry. The waves propagate along the x-direction in a Cartesian coordinate system

To avoid complexity we assume the propagation of wave is in x-direction of the Cartesian system and zero spatial variation in y-direction.

$$E(x, y, z) = E(z)e^{j\beta x} \tag{2.18}$$

Where, $\beta = k_x$ which is propagation constant.

Now inserting the value of E the wave equation will be:

$$\frac{\partial^2 E(z)}{\partial z^2} + (k_0^2\varepsilon - \beta^2)\, E = 0 \tag{2.19}$$

Similarly we can derive the equation for the magnetic field H. The field E and H can be decomposed in Cartesian coordinate system as:

$$E = E_x.\overrightarrow{a_x} + E_y.\overrightarrow{a_y} + E_z.\overrightarrow{a_z} \tag{2.20}$$

$$H = H_x.\overrightarrow{a_x} + H_y.\overrightarrow{a_y} + H_z.\overrightarrow{a_z} \tag{2.21}$$

For harmonic dependence $\frac{\partial}{\partial t} = -j\omega$ and by solving the Ampere's law and Faraday's law we get:

$$\frac{\partial E_z}{\partial y} - \frac{\partial E_y}{\partial z} = j\omega\mu_0 H_x \tag{2.22}$$

$$\frac{\partial E_x}{\partial z} - \frac{\partial E_z}{\partial x} = j\omega\mu_0 H_y \tag{2.23}$$

$$\frac{\partial E_y}{\partial x} - \frac{\partial E_x}{\partial y} = j\omega\mu_0 H_z \tag{2.24}$$

$$\frac{\partial H_z}{\partial y} - \frac{\partial H_y}{\partial z} = -j\omega\varepsilon_0\varepsilon E_x \tag{2.25}$$

$$\frac{\partial H_x}{\partial z} - \frac{\partial H_z}{\partial x} = -j\omega\varepsilon_0\varepsilon E_y \tag{2.26}$$

$$\frac{\partial H_y}{\partial x} - \frac{\partial H_x}{\partial y} = -j\omega\varepsilon_0\varepsilon E_z \tag{2.27}$$

As the propagation is in x-direction in the form of $e^{j\beta x}$ which follows that $\frac{\partial}{\partial x} = -j\beta$. The homogeneity in y-direction makes $\frac{\partial}{\partial y}$=0. So the equations will be simplified as:

$$-\frac{\partial E_y}{\partial z} = j\omega\mu_0 H_x \tag{2.28}$$

$$\frac{\partial E_x}{\partial z} - j\beta E_z = j\omega\mu_0 H_y \tag{2.30}$$

$$j\beta E_y = j\omega\mu_0 H_z \tag{2.31}$$

$$\frac{\partial H_y}{\partial z} = j\omega\varepsilon_0\varepsilon E_x \tag{2.32}$$

$$\frac{\partial H_x}{\partial z} - j\beta H_z = j\omega\varepsilon_0\varepsilon E_y \tag{2.33}$$

$$j\beta H_y = - j\omega\varepsilon_0\varepsilon E_z \tag{2.34}$$

The above equation solutions can be categorized depending on the polarization as, Transverse Magnetic (TM) mode and Transverse Electric (TE) mode. The equations for TM mode are:

$$E_x = -j \frac{1}{\omega\varepsilon_0\varepsilon} \frac{\partial H_y}{\partial z} \tag{2.35}$$

$$E_z = - \frac{\beta}{\omega\varepsilon_0\varepsilon} H_y \tag{2.36}$$

Therefore the wave equation for TM polarized wave is:

$$\frac{\partial^2 H_y}{\partial z^2} + (k_0^2 - \beta^2) H_y = 0 \tag{2.37}$$

Similarly, TE polarized equation:

$$H_x = j \frac{1}{\omega\mu_0} \frac{\partial E_y}{\partial z} \tag{2.38}$$

$$H_z = \frac{\beta}{\omega\mu_0} E_y \tag{2.39}$$

Hence, the TE wave equation will be:

$$\frac{\partial^2 E_y}{\partial z^2} + (k_0^2 \varepsilon - \beta^2)\, E_y = 0 \tag{2.40}$$

2.3 SPP at single interface:

The simplest form of SPP propagation is at single interface, between dielectric and metal with ε_1 as positive dielectric constant for the dielectric and ε_2 as negative dielectric constant for metal. For metal the bulk Plasmon frequency will be ω_p and the amplitude decays perpendicular to the z-direction.

For the TM solutions in both spaces: metal and dielectric will be for $z > 0$

$$H_z(z) = A_2 e^{j\beta x}\, e^{-k_2 z} \tag{2.41}$$

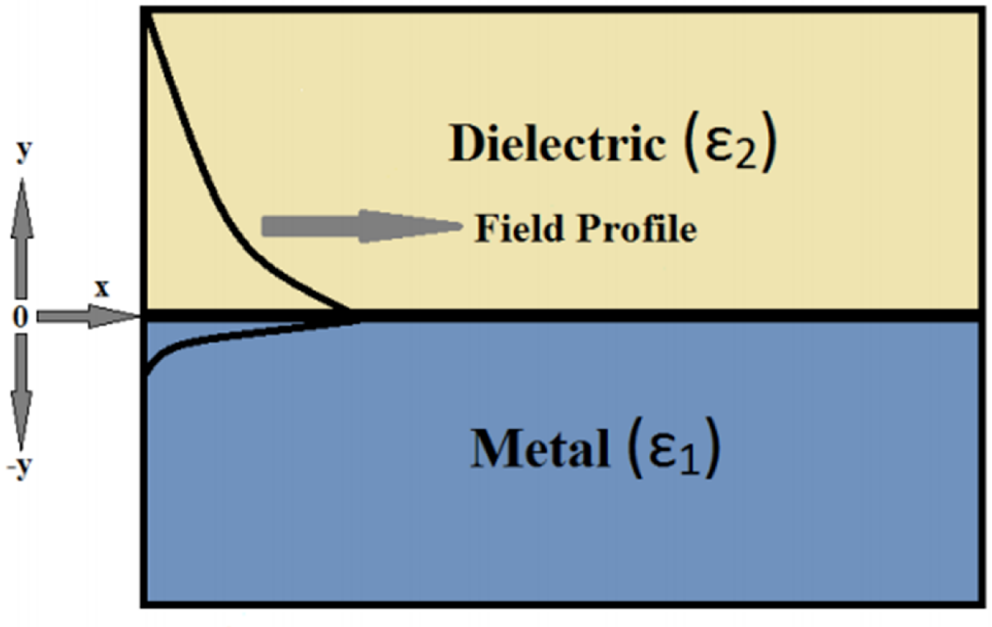

Figure 2.2: SPP at the Single interface.

$$E_x(z) = jA_2\frac{1}{\omega\varepsilon_0\varepsilon_2} k_2\, e^{j\beta x}\, e^{-k_2 z} \tag{2.42}$$

$$E_z(z) = -A_1\frac{\beta}{\omega\varepsilon_0\varepsilon_2} e^{j\beta x}\, e^{-k_2 z} \tag{2.43}$$

And for $z < 0$,

$$H_y(z) = A_1\, e^{j\beta x}\, e^{k_1 z} \tag{2.44}$$

$$E_x(z) = -jA_1\ \frac{1}{\omega\varepsilon_0\varepsilon_1} k_1\, e^{j\beta x}\, e^{k_1 z} \tag{2.45}$$

$$E_x(z) = -A_1\ \frac{\beta}{\omega\varepsilon_0\varepsilon_1} e^{j\beta x}\, e^{k_1 z} \tag{2.46}$$

The continuity of H_y and $\varepsilon_i E_z$ at the metal dielectric interface gives $A_1 = A_2$ and

$$\frac{k_2}{k_1} = -\frac{\varepsilon_2}{\varepsilon_1} \tag{2.47}$$

The surface wave exists at the metal dielectric interface with opposite sign of their real dielectric permittivities. So, we can write

$$k_1^2\varepsilon = \beta^2 + k_0^2\varepsilon_1 \tag{2.48}$$

$$K_2^2\varepsilon = \beta^2 + k_0^2\varepsilon_2 \tag{2.49}$$

The dispersion relation of SPPs propagation is

$$B = k_0 \sqrt{\frac{\varepsilon_1 \varepsilon_2}{\varepsilon_1 + \varepsilon_2}} \tag{2.50}$$

The TE surface modes can be expressed as:

$$E_y(z) = A_2 e^{j\beta x} e^{-k_2 z} \tag{2.51}$$

$$H_x(z) = -jA_2 \frac{1}{\omega\mu_0} k_2 e^{j\beta x} e^{-k_2 z} \tag{2.52}$$

$$H_z(z) = -A_2 \frac{\beta}{\omega\mu_0} e^{j\beta x} e^{-k_2 z} \tag{2.53}$$

For $z > 0$, and

$$E_y(z) = A_1 e^{j\beta x} e^{k_1 z} \tag{2.54}$$

$$H_x(z) = jA_1 \frac{1}{\omega\varepsilon_0\varepsilon_1} k_1 e^{j\beta x} e^{k_1 z} \tag{2.55}$$

$$H_z(z) = A_1 \frac{\beta}{\omega\varepsilon_0\varepsilon_1} e^{j\beta x} e^{k_1 z} \tag{2.56}$$

For, $z < 0$. The continuity of E_y and H_x requires:

$$A_1 (k_1 + k_2) = 0 \tag{2.57}$$

The surface requires the real part of k_1 and k_2 should be greater than zero for confinement. This will be satisfied if $A_1 = A_2 = 0$. Therefore no surface modes for TE polarization. SPP only exist for TM polarization.

2.4 SPP at double interface:

Two mostly used double interface configurations of SPP waveguides are: Metal-Dielectric-Metal (MDM) and Dielectric-Metal-Dielectric (DMD). In these cases SPPs are formed on both interfaces. When the distance is shorter than decay distance, it forms coupled mode of SPP. This coupled mode of propagation can also be sub-divided into even and odd modes, as shown in the figure:

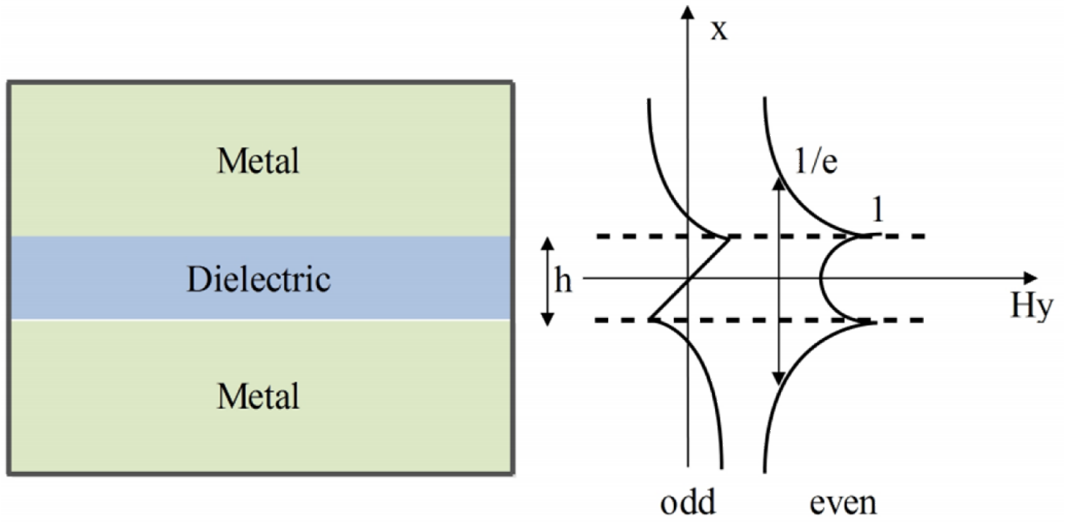

Figure 2.3: SPP at the double interface

Chapter 3

Material Modeling Within Optical Range

3.1 Introduction:

Metals act as perfect conductors for low frequencies, owing to their lack of dispersive behavior for long wavelengths. But for higher frequencies for example, the optical range, the behavior is quite the opposite, since there is field inside the metal, it behaves as dispersive material. And for frequencies higher than optical range metal acts as dielectric material. Properties of SPPs depend highly on the material response to light. In this chapter we will be studying about the material supporting SPP, descriptions and derivations of different models for describing the behavior of metal in the presence of light.

Now in presence of an external oscillating electromagnetic field, three vectors can determine the behavior of any material. Such as: D (electrical flux density), E (electric field intensity) and P (polarization density). In frequency domain the corresponding equation will be:

$$D(\omega) = \varepsilon(\omega)\, E(\omega) \tag{3.1}$$

$$P(\omega) = \varepsilon_0\, \chi(\omega)\, E(\omega) \tag{3.2}$$

$$D(\omega) = \varepsilon_0\, E(\omega) + P(\omega) \tag{3.3}$$

Combining these equations we get:

$$D(\omega) = \varepsilon_0\, E(\omega)\, (1 + \chi(\omega)) \tag{3.4}$$

where χ is the electric susceptibility which measures how easily it is polarized in response to an applied electric field, and it is a dimensionless quantity.

Finally the relation between the permittivity and susceptibility is:

$$E(\omega) = \varepsilon_0(1 + \chi(\omega)) \tag{3.5}$$

So the relative permittivity will be:

$$E_r = 1 + \chi(\omega) \tag{3.6}$$

For linear isotropic materials such as glass this above values become simple. But for a dispersive material, the frequency dependent permittivity and susceptibility should be modeled perfectly for getting the perfect response of the material for certain electromagnetic excitation. Some widely used material models are Drude model, Lorentz model, Debye model and Lorentz-Drude model.

3.2 Different Material Models:

3.2.1 The Drude model:

The Drude model of electrical conduction was first developed by Paul Drude. In his model he described the metal as a volume filled with stationary positive ions, immersed in a gas of electrons following the kinetic theory of gases. These electrons are free to move inside the metal without any interaction with each other. The electrons in a metal are subjected to two forces, such as,

1. Driving force F_d

2. Damping force F_g

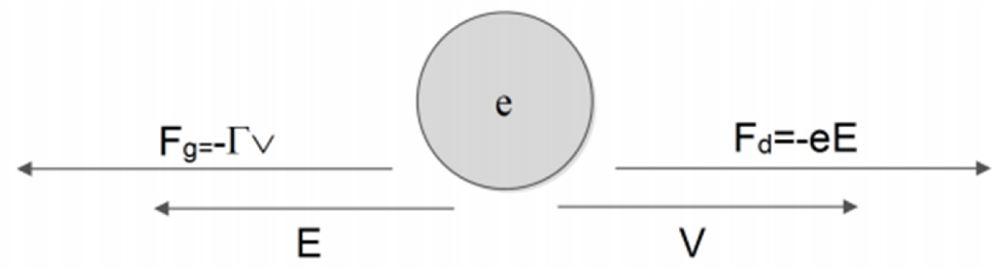

Figure 3.1: Drude model

The driving force and the damping force can be expressed as:

$$F_d = qE = -eE \tag{3.7}$$

$$F_g = -\Gamma \upsilon \tag{3.8}$$

As the two forces are opposite of each other, the resultant force will be

$$F = F_d - F_g \tag{3.9}$$

From Newton's first law of motion we can write:

$$mr'' = -eE + \Gamma r' \tag{3.10}$$

where,

m = the mass of an electron

Γ =is the damping constant in Newton second per meter

r = the displacement in meter

v = the velocity of the electron

q = the electrons charge

the prime indicates differentiation order with respect to time

For time harmonic electric field and time harmonic displacement the equation will be:

$$E(t) = E_0 e^{-j\omega t} \leftrightarrows E(\omega) \tag{3.11}$$

$$r(t) = R_0 e^{-j\omega t} \leftrightarrows R(\omega) \tag{3.12}$$

From equaion 3.10 the frequency domain form will be:

$$mR''(\omega) - \Gamma mR'(\omega) + eE(\omega) = 0 \tag{3.13}$$

The derivatives of frequency domain will give:

$$-m\omega^2 R''(\omega) - j\omega\Gamma mR'(\omega) + eE(\omega) = 0 \tag{3.14}$$

Simplifying the above equation, the displacement R will give

$$R(\omega) = \frac{-e}{m(j\Gamma\omega - \omega^2)} E(\omega) \tag{3.15}$$

The polarization for n number of electrons will be:

$$P(\omega) = -neR(\omega) \tag{3.16}$$

or,

$$P(\omega) = \frac{-ne^2}{m(j\Gamma\omega - \omega^2)} E(\omega) \tag{3.17}$$

An expression for the susceptibility can also be obtained from the above equation and that will be:

$$\frac{P(\omega)}{\varepsilon_0 E(\omega)} = \frac{-ne^2}{\varepsilon_0 m(j\Gamma\omega - \omega^2)} = \chi(\omega) \tag{3.18}$$

Now substituting this value in equation 3.6 we get

$$E_r(\omega) = 1 + \frac{-ne^2}{\varepsilon_0 m(j\Gamma\omega - \omega^2)} \tag{3.19}$$

if we consider ω_p as the plasma frequency that will provide:

$$\omega_p{}^2 = \frac{ne^2}{\varepsilon_o m} \tag{3.20}$$

So, the frequency dependent flux density will be

$$D(\omega) = \varepsilon_0 (1 + \frac{\omega_p^2}{j\Gamma\omega - \omega^2}) E(\omega) \tag{3.21}$$

For low frequency, the term $\Gamma\omega << 1$, therefore, the dispersive relation can be reduced to:

$$D(\omega) = \varepsilon_0 (1 - \frac{\omega_p^2}{\omega^2}) E(\omega) \tag{3.22}$$

3.2.2 The Lorentz Model:

The Lorentz model can be useful in studying the atom field interaction. In this model, Lorentz modeled atom as a mass (nucleus) interacting with another mass (electron). In Lorentz model the electrons are assumed to be bound to the nucleus and not free. So there is a restoring force acting between them which is denoted by F_r.

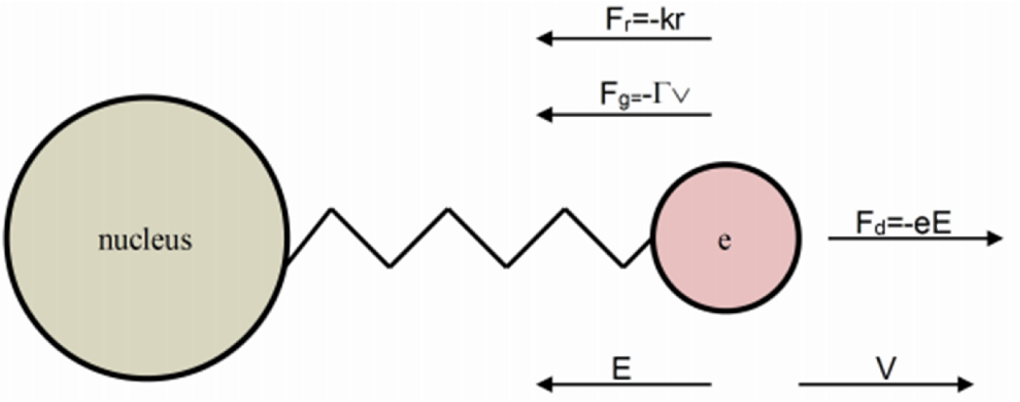

Figure 3.2: Lorentz model

The restoring force can be written as:

$$F_r = -k_r \tag{3.23}$$

Where, k is the spring constant in Newtons per meter.

From the law of motion we can see that:

$$mr'' + m\Gamma r' + mkr + eE = 0 \tag{3.24}$$

In frequency domain the above equation becomes:

$$R(\omega)(m\omega_0^2 + j\omega m\Gamma - m\omega^2) - eE(\omega) \tag{3.25}$$

Considering the natural frequency $\omega_0 = \sqrt{\frac{k}{m}}$ we get

$$R(\omega) = \frac{-e}{m(\omega_0^2 + j\Gamma\omega - \omega^2)} E(\omega) \tag{3.26}$$

So the susceptibility can be found as:

$$\frac{P(\omega)}{\varepsilon_0 E\omega} = \frac{-ne^2}{\varepsilon_0 m(\omega_0^2 + j\Gamma\omega - \omega^2)} = \chi(\omega) \tag{3.27}$$

So from the equation 3.4 the expression for D can be expressed in frequency domain as:

$$D(\omega) = \varepsilon_0\left(1 + \frac{\omega_p^2}{(\omega_0^2 + j\Gamma\omega - \omega^2)}\right) E(\omega) \tag{3.28}$$

3.2.3 The Lorentz Drude model:

In the Lorentz Drude model the electrons of two types oscillate inside metal and they contribute to permittivity. The free electrons contribute a permittivity of the Drude model, and the bound electrons contribute a permittivity of the Lorentz model. The permittivity in the LD model is given by:

$$\varepsilon = \varepsilon_{free} + \varepsilon_{bound} \tag{3.29}$$

where

$$\varepsilon_{free} = 1 + \frac{\omega_p}{j\Gamma\omega - \omega^2} \tag{3.30}$$

$$\varepsilon_{bound} = \frac{\omega_p}{(\omega_0 + j\Gamma\omega - \omega^2)} \tag{3.31}$$

Therefore combining both the model together the electric field density D in frequency domain will be:

$$D(\omega) = \varepsilon_0\left(1 + \frac{\omega_p}{j\Gamma\omega - \omega^2} + \frac{\omega_p}{(\omega_0 + j\Gamma\omega - \omega^2)}\right) E(\omega) \tag{3.32}$$

3.2.4 The Debye Model:

According to Debye model materials are made of electric dipoles therefore when the material is put into field the dipoles rearrange themselves according to the applied field with some relaxation time. The strength of polarization depends on the frequency of the electric field. For slow frequency there will be strong polarization and for fast frequency weak polarization. It can also be said that materials with short relaxation time have strong polarization and materials with long relaxation time has low or no polarization. Metals have very short relaxation time, hence polarization in metals is strong. If a DC electric field is applied to a dielectric, the polarization takes some time to follow the electric field. At steady state, it will be:

$$P(t) = P_{\infty}(1 - e^{\frac{-t}{\tau}}) \tag{3.33}$$

Where P(t) is instantaneous polarization,

P_{∞} is the polarization in the steady state τ is the time constant.

The derivation of the above equation will be

$$\frac{dP(t)}{dt} = \frac{1}{\tau} P_{\infty} e^{\frac{-t}{\tau}} \tag{3.34}$$

Now combining both the equations we get:

$$P(t) = P_{\infty} - \tau \frac{dP(t)}{dt} \tag{3.35}$$

As $P_{\infty} = \varepsilon_0 (\varepsilon - 1) E(t)$ so the equation will be reduced to

$$P(t) = \varepsilon_0 (\varepsilon - 1) E(t) - \tau \frac{dP(t)}{dt} \tag{3.36}$$

In frequency domain the equation will be:

$$\varepsilon_0 (\varepsilon - 1) E(\omega) = P(\omega) + j\omega t\, P(\omega) \tag{3.37}$$

or,

$$P(\omega) = \frac{\varepsilon_0(\varepsilon-1)}{1+j\omega\tau} E(\omega) \tag{3.38}$$

The susceptibility can be expressed as:

$$\frac{E-1}{1+j\omega\tau} = \frac{P(\omega)}{\varepsilon_0 E(\omega)} = \chi(\omega) \tag{3.39}$$

The relative permittivity will be:

$$E_r(\omega) = \chi(\omega) + 1 = \frac{\varepsilon-1}{1+j\omega\tau} + 1 \tag{3.40}$$

For the permittivity function to fit in the range from 0 frequency to infinity frequency, the boundary conditions are $\varepsilon_r(0) = \varepsilon_s$ and $\varepsilon_r(\infty) = \varepsilon_\infty$

Therefore, the relation can be modified to:

$$E(\omega) = \varepsilon_\infty + \frac{\varepsilon_s-\varepsilon_\infty}{1+j\omega\tau} \tag{3.41}$$

To take into account the material losses that SPPs encounter, another term is added with the permittivity of metal. So the above equation can be expanded to:

$$\varepsilon(\omega) = \varepsilon_\infty + \frac{\varepsilon_s-\varepsilon_\infty}{1+j\omega\tau} - j\frac{\sigma}{\omega\varepsilon_0} \tag{3.42}$$

The Debye model can also be expressed in real and imaginary terms:

$$\varepsilon_r(\omega) = \varepsilon'(\omega) - j\varepsilon''(\omega) \tag{3.43}$$

where

$$\varepsilon'(\omega) = = \varepsilon_\infty + \frac{\varepsilon_s-\varepsilon_\infty}{1+\omega^2\tau^2} \tag{3.44}$$

and

$$\varepsilon''(\omega) = \varepsilon_\infty + \frac{(\varepsilon_s-\varepsilon_\infty)\omega\tau}{1+\omega^2\tau^2} + \frac{\sigma}{\omega\varepsilon_0} \tag{3.45}$$

3.3 Material Dispersion:

Dispersion can be defined as the variation of the propagating waves wavelength with frequency. It is also sometimes defined as the variation of propagating waves wave number $k = \frac{2\pi}{\lambda}$ with angular frequency, $\omega = 2\pi f$. So the one dimensional wave equation will be:

$$\frac{\partial^2 u}{\partial t^2} = \upsilon^2 \frac{\partial^2 u}{\partial x^2} \tag{3.46}$$

Where,

$\upsilon^2 = \frac{1}{\mu\varepsilon}$ The solution of the above wave equation can be written in phasor form as

$$u(x, t) = e^{j(\omega t - kx)} \tag{3.47}$$

Now putting this value in the wave equation we get

$$(j\omega)^2 e^{j(\omega t - kx)} = v^2(-jk)^2 e^{j(\omega t - kx)} \tag{3.48}$$

Finally from this equation we get:

$$K = \pm \frac{\omega}{\upsilon} \tag{3.49}$$

The + sign is for -x directed wave propagation and - sign is for +x directed wave propagation. The magnetic flux density and electric flux density for dispersive medium are:

$$D(\omega) = \varepsilon(\omega) E \tag{3.50}$$

$$B(\omega) = \mu(\omega) H \tag{3.51}$$

Here both $\varepsilon(\omega)$ and $\mu(\omega)$ are frequency dependent functions.

Chapter 4

Finite-Difference-Time-Domain method

4.1 The Yee algorithm:

Yee algorithm is used in FDTD simulations.

The original proposal was intended for homogeneous, isotropic and lossless media based on discretizing the volume into cells in Cartesian coordinates. The Yee algorithm solves for both electric and magnetic fields using the coupled Maxwell's time dependent curl equations, rather than solving for the electric field alone (or the magnetic field alone) with a wave equation.

The method begins with two of Maxwell's equations:

$$D\frac{\partial \vec{H}}{\partial t} = \frac{1}{\mu}\nabla \times \vec{E} \tag{4.1}$$

$$D\frac{\partial \vec{E}}{\partial t} = \frac{1}{\varepsilon}\nabla \times \vec{H} \tag{4.2}$$

The electric and magnetic fields are three dimensional vectors. Each equation can be converted into three coupled scalar first order differential equations. The derivatives are both in space and time. The curl operations of equations 4.1 and equation 4.2 yields the following six equations in Cartesian coordinates:

$$\frac{\partial E_z}{\partial y} - \frac{\partial E_y}{\partial z} = \mu \frac{\partial H_x}{\partial t} \tag{4.3}$$

$$\frac{\partial E_x}{\partial z} - \frac{\partial E_z}{\partial x} = \mu \frac{\partial H_y}{\partial t} \tag{4.4}$$

$$\frac{\partial E_y}{\partial x} - \frac{\partial E_x}{\partial y} = \mu \frac{\partial H_z}{\partial t} \tag{4.5}$$

$$\frac{\partial H_z}{\partial y} - \frac{\partial H_y}{\partial z} = \varepsilon \frac{\partial E_x}{\partial t} \tag{4.6}$$

$$\frac{\partial H_x}{\partial z} - \frac{\partial H_z}{\partial x} = \varepsilon \frac{\partial E_y}{\partial t} \tag{4.7}$$

$$\frac{\partial H_y}{\partial x} - \frac{\partial H_x}{\partial y} = \varepsilon \frac{\partial E_z}{\partial t} \tag{4.8}$$

Then the scalar differential equations are converted into difference equations. In order to do that, discretization is required for both space and time. For space discretization, Yee visualized the field components arranged within a unit cell (voxel). The electric field components are stored on the corresponding cell edges, while the magnetic field components are stored on the corresponding face centers.

The fields are located in a way where each E component is surrounded by four H components and vice versa, which leads to a spatially coupled system of field circulations corresponding to the law of Faraday and Ampere. The figure 4.1 shows the Yee's spatial grid.

Considering a two dimensional TM (Transverse Magnetic) polarized field case,

$$\frac{\partial E_x}{\partial t} = \frac{1}{\varepsilon} \frac{\partial H_z}{\partial y} \tag{4.9}$$

$$\frac{\partial E_y}{\partial t} = \frac{1}{\varepsilon}\frac{\partial H_z}{\partial x} \tag{4.10}$$

$$\frac{\partial H_z}{\partial t} = \frac{1}{\mu}\left(\frac{\partial E_x}{\partial y} - \frac{\partial H_y}{\partial x}\right) \tag{4.11}$$

Central difference approximation is applied in each of the equations 4.9, 4.10 and 4.11 which finally conclude in a spatial scalar difference equations in 4.12, 4.13 and 4.14.

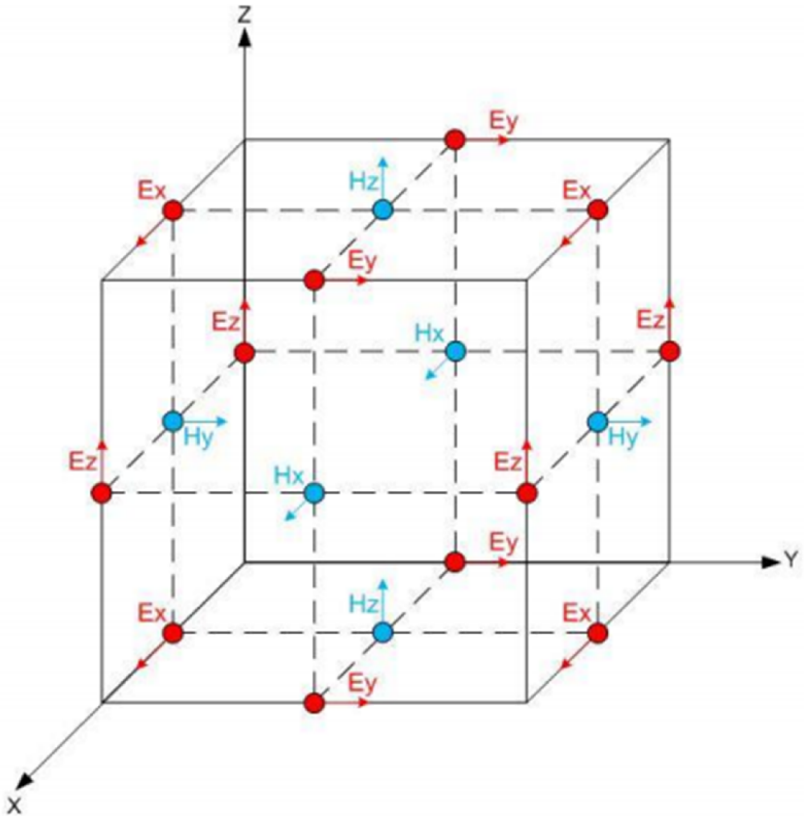

Figure 4.1: Yee's spatial grid

$$\frac{\partial E_x}{\partial t} = \frac{1}{\varepsilon}\frac{H_z(i,j) - H_z(i,j-1)}{\Delta y} \tag{4.12}$$

$$\frac{\partial E_y}{\partial t} = \frac{1}{\varepsilon}\frac{H_z(i,j) - H_z(i-1,j)}{\Delta x} \tag{4.13}$$

$$\frac{\partial H_z}{\partial t} = \frac{1}{\mu}\left(\frac{E_x(i,j+1) - E_x(i,j)}{\Delta y} - \frac{E_y(i+1,j) - E_y(i,j)}{\Delta x}\right) \tag{4.14}$$

In order to consider the time derivatives, the time axis is to be considered as shown in the figure. The Electric and Magnetic field are mapped half a step apart along the time axis. Again applying the central difference approximation the equations 4.12, 4.13 and 4.14 become:

$$\frac{E_x^{n+1}(i+\frac{1}{2},j) - E_x^{n}(i+\frac{1}{2},j)}{\Delta t} = \frac{1}{\varepsilon}\frac{H_z^{n+\frac{1}{2}}(i+\frac{1}{2},j) - H_z^{n+\frac{1}{2}}(i+\frac{1}{2},j-\frac{1}{2})}{\Delta y}$$

$$\frac{E_y^{n+1}(i,j+\frac{1}{2},) - E_y^{n}(i,j+\frac{1}{2})}{\Delta t} = -\frac{1}{\varepsilon}\frac{H_z^{n+\frac{1}{2}}(i+\frac{1}{2},j+\frac{1}{2}) - H_z^{n+\frac{1}{2}}(i-\frac{1}{2},j+\frac{1}{2})}{\Delta y}$$

$$\frac{H_z^{n+\frac{1}{2}}(i+\frac{1}{2},j+\frac{1}{2}) - H_z^{n-\frac{1}{2}}(i+\frac{1}{2},j+\frac{1}{2})}{\Delta t} = -\frac{1}{\mu}\left(\frac{E_x^{n+1}(i+\frac{1}{2},j+1,) - E_x^{n}(i+\frac{1}{2},j)}{\Delta y} - \frac{E_y^{n}(i+1,j+\frac{1}{2},) - E_y^{n}(i,j+\frac{1}{2})}{\Delta x}\right)$$

Each field component depends on the field of previous time step itself and the surrounding component in Yee's algorithm.

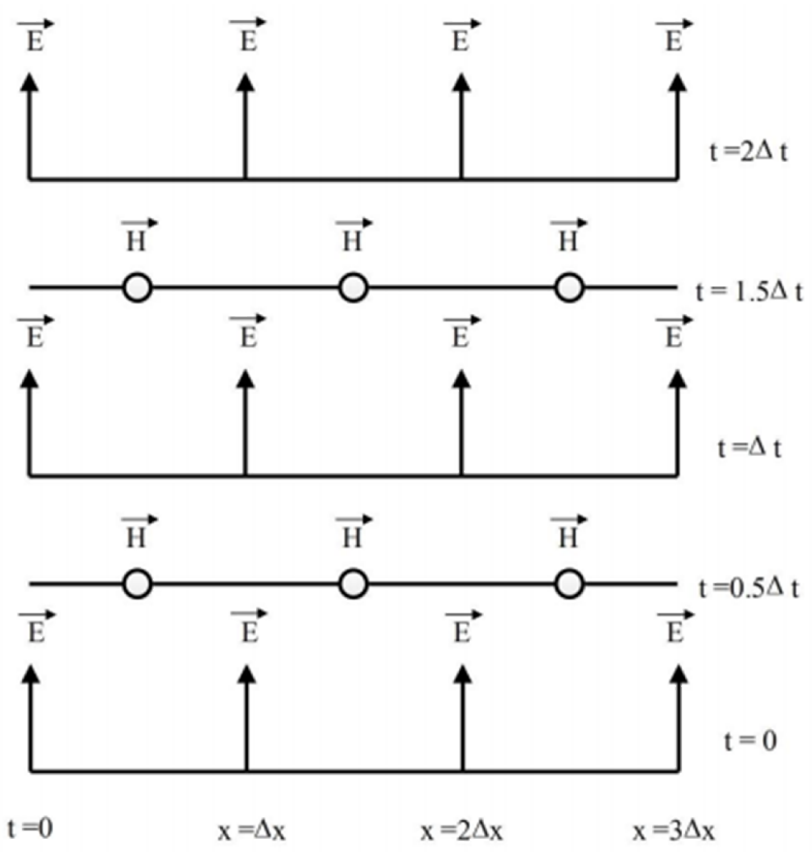

Figure 4.2: The temporal scheme of FDTD method.

Numerical stability of the Yee algorithm is required to be ensured. In an unstable algorithm the computed magnitude of electric and magnetic field components will gradually increase without limit with the progression of simulation. To guarantee numerical stability, the EM field's propagation should not be faster than the allowed limit which is imposed by the phase velocity within the material. This is done by limiting time step Δt using the Courant-Friedrichs-Lewy criterion for the general Yee FDTD grid as follows:

$$\Delta t \leq \left\{ \frac{1}{\upsilon_p \sqrt{\frac{1}{\Delta x^2} + \frac{1}{\Delta y^2} + \frac{1}{\Delta z^2}}} \right\} \tag{4.15}$$

where Δx, Δy and Δz indicate the spatial Cartesian grid increments.

4.2 Absorbing Boundary Condition (ABC)

In FDTD method, a space of theoretically infinite extent with a finite computational cell is simulated due to limited computer resources. The boundary is said to be ideally absorbing, without any non-physical reflection back to the region. To accomplish this, a number of boundary conditions such as Berenger's perfectly matched layer (PML), have been proposed. An artificial layer surrounds the computational domain so that most of the outgoing waves are absorbed. The electromagnetic fields are made to attenuate rapidly until they become equal to zero, so that they do not produce any reflections.

4.3 Material Dispersion in FDTD:

The material is said to be dispersive when the permittivity and permeability of a material are functions of frequency. In reality the assumption of constant relative permittivity is not absolutely correct. Because by doing so, instantaneous polarization of charge within a material is being assumed.

In order to exploit the realistic wave propagation, dispersive FDTD techniques become necessary.

The existing FDTD based algorithms for the analysis of material dispersion can be categorized into three types:

1) the auxiliary differential equation (ADE),
2) the Z-transform methods, and
3) methods base on discrete convolution of the dispersion relation or the recursive convolution (RC) method.

We will highlight on the ADE dispersive FDTD method as we have applied in material modeling. The other methods will also be briefly discussed.

4.3.1 The Auxiliary Differential Equation (ADE):

Taflove introduced the auxiliary differential equation to the FDTD modeling in order to integrate the dispersion relation into the model. The dispersion relation is converted from frequency domain to time domain through Fourier transform in the basic step of the procedure. The Fourier transform results in a relationship between the new E field value and the previous E and D values, which can be added to the algorithm to update the E fields. The new algorithm with ADE becomes

$$\frac{\partial}{\partial t}H_z = -\frac{1}{\mu}\left(\frac{\partial E_x}{\partial y} - \frac{\partial E_y}{\partial x}\right) \tag{4.16}$$

$$\frac{\partial}{\partial t}D_x = \frac{\partial H_z}{\partial y} \tag{4.17}$$

In order to get the function relating D to E in a dispersive medium, we start with

$$D(\omega) = \varepsilon_0 \frac{\sigma}{j\omega} E(\omega) \tag{4.18}$$

Multiplying by jω

$$j\omega D(\omega) = \varepsilon_0 \sigma E(\omega) \tag{4.19}$$

Applying the Fourier transform in equation 4.19

$$\frac{d}{dt}D(t) = \varepsilon_0 \sigma E(t) \tag{4.20}$$

Discretizing equation 4.20 equation using forward difference method

$$\frac{D^n - D^{n-1}}{\Delta t} = \varepsilon_0 \sigma E(t) \tag{4.21}$$

Finally solving for E, we find the update equation

$$E^n = \frac{D^n - D^{n-1}}{\varepsilon_0 \sigma \Delta t} \tag{4.22}$$

4.3.2 The Z-transform Model:

The Z-transform is a faster method compared to ADE method. Sullivan used the Z-transform method for the first time in order to introduce the dispersion relation into the FDTD algorithm.

The Z-transform of the equation

$$D(\omega) = \varepsilon(\omega) E(\omega) \tag{4.23}$$

is

$$D(z) = \varepsilon(z) \Delta t E(z) \tag{4.24}$$

Multiplying by $(1 - z^{-1})$, we find

$$D(z)(1 - z^{-1}) = \varepsilon_o \sigma E(z) \tag{4.25}$$

or,

$$D(z) - z^{-1} D(z) = \varepsilon_o \sigma E(z) \tag{4.26}$$

Performing inverse z-transform

$$D_n - D_{n-1} = \varepsilon_o \sigma \Delta t E^n \tag{4.27}$$

Finally, for solving E from equation 4.28, we find

$$E^n = \frac{D^n - D^{n-1}}{\varepsilon_0 \sigma \Delta t} \tag{4.28}$$

which is same as the final update equation derived by ADE method.

4.3.3 Piecewise Linear Recursive Convolution Method:

Luebbers et al. formulated the first frequency dispersive FDTD algorithm using the recursive convolution (RC) scheme. Later it became piecewise linear recursive convolution(PLRC) method [32]. Initially developed for Debye media [33], the approach was later extended for the study of wave propagation in a Drude material [34], N-th order dispersive media [35], an anisotropic magneto-active plasma [36], ferrite material [37]and the bi-isotropic/chiral media [38] [39].

The RC approach, typically being faster and having required fewer computer memory resources than other approaches, is usually less accurate. But in case of multiple pole mediums, it is easier to follow the RC approach. In the initial derivation of PLRC method for a linear dispersive medium, the relation between electric flux density and electric field intensity is expressed as:

$$D(t) = \varepsilon_o \varepsilon_\infty E(t) + \varepsilon_0 \int_0^t E(t-\tau)\chi(\tau)d\tau \tag{4.29}$$

which can be discretized as:

$$D^n = \varepsilon_o \varepsilon_\infty E^n + \varepsilon_0 \int_0^{n\Delta t} E(n\Delta t-\tau)\chi(\tau)d\tau \tag{4.30}$$

The PRC method is further preceded from this basing discrete equation.

4.4 The General Algorithm:

The derivation of equations for multi-pole dispersion relation is more difficult compared to the single pole-pair dispersion relation. For example, for six-pole Lorentz-Drude dispersion the required derivation process is lengthy. Additionally, the memory required for computation is also vast. There are various methods proposed by researchers regarding this topic such as Taflove's matrix inversion method, Multi-term dispersion by Okoniewski, etc. However Alsunaidi and Al-Jabr proposed a general algorithm technique which solves various problems regarding previous

methods. The major advantage of this technique is that it requires only one algorithm for any dispersion relation. The dispersive relation has the general form as:

$$D\ (\omega)\ =\ \varepsilon\ (\omega)\ E\ (\omega) \tag{4.31}$$

which can be expressed in terms of summation of poles

$$D\ (\omega) = \varepsilon_o\varepsilon_\infty E(\omega) + \sum_i^N P_i(\omega) \tag{4.32}$$

where N is the number of poles. Applying Fourier transform, this equation becomes

$$D^{n+1} = \varepsilon_o\varepsilon_\infty E^{n+1} + \sum_i^N P_i^{n+1} \tag{4.33}$$

or,

$$E^{n+1}\ =\ \frac{D^{n+1}-\sum_i^N P_i^{n+1}}{\varepsilon_0\varepsilon_\infty} \tag{4.34}$$

This term P_i can be any form of dispersion relation such as the Debye, the Drude or just the conductivity term. This is the final solved equation for E.

Chapter 5

Comparison of waveguides using different materials

5.1 Simulation model developing

The simulation model we have developed is based on the FDTD method [40]. We have used the general auxiliary differential equation (ADE) based FDTD [41] approach in order to incorporate the frequency dependent dispersion property of the constituent materials. This algorithm is useful for the simulation of materials with different dispersive properties. The perfectly matched layer [42] has been implemented at all the boundaries in order to prevent back reflections and artificially creating a substrate of infinite dimension.

Considering the material dispersion, the frequency-dependent electric flux density can be given as

$$D(\omega) = \varepsilon_0 \varepsilon_\infty E(\omega) + P(\omega) \tag{5.1}$$

The general Lorentz model is given by

$$P(\omega) = \frac{a}{b + jc\omega - d\omega^2} \tag{5.2}$$

which can be written in time-domain through inverse Fourier transform as

$$bP(t) + cP'(t) + dP''(t) = aE(t) \tag{5.3}$$

The FDTD solution for the first order polarization of Eq. (3) can be expressed as

$$P^{n+1} = C_1 P^n + C_2 P^{n-1} + C_3 E^n \tag{5.4}$$

where, $C_1 = \frac{4d - 2b\Delta t^2}{2d + c\Delta t}$, $C_2 = \frac{-2d - c\Delta t}{2d + c\Delta t}$ and $C_3 = \frac{2a\Delta t^2}{2d + c\Delta t}$

The values of C_1, C_2 and C_3 depend on the material under consideration. Finally the electric field intensity becomes,

$$E^{n+1} = \frac{D^{n+1} - \sum_{i=1}^{N} P_i^{n+1}}{\varepsilon_0 \varepsilon_\infty} \tag{5.5}$$

where, N is the number of poles and D^{n+1} is the update value of the electric flux density calculated using FDTD algorithm.

5.2 Verification of the developed model

In order to verify our developed simulation model we have simulated one dimensional dispersive material using the parameters given by Taflove [43]. The obtained result has been compared with the result provided by Taflove [43]and we have found an excellent agreement. The parameters given in the book of Taflove [43] are as follows,

$\varepsilon_s = 5.25, \varepsilon_\infty = 2.25, \omega_0 = 4 \times 10^{14} (rad/sec)$ and $\delta = 2 \times 10^9 (rad/sec)$.

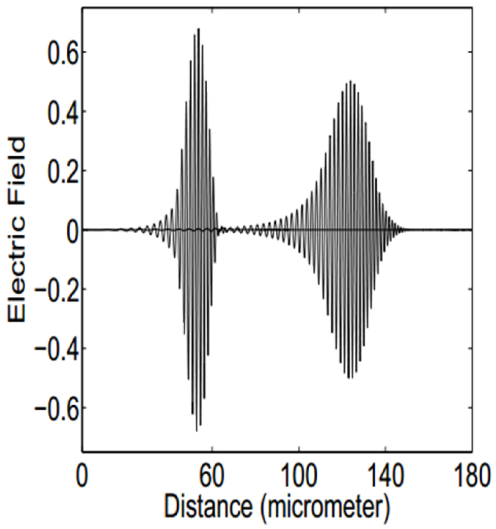

Figure 5.1: Simulated result using parameters given in the book of Taflove

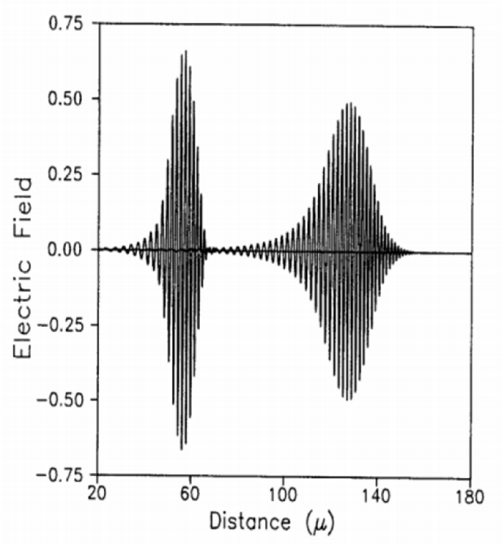

Figure 5.2: Result given in the book of Taflove

5.3 SPP propagation through different Nano-waveguides

5.3.1 Material properties used for simulations

The modeling parameters used for simulations are taken from different resources.

The modeling parameters for Ag that we have used, have been determined by Rakic et al. [26]. The dispersion properties for AlGaAs and GLS, have been determined by M. Alsunaidi et al. [44] and R H Sagor [45] respectively. The dispersion properties for Cu_2O, SiGe [46] and AlAs, Al_2O_3 [47] have been determined by Md. Ghulam Saber and R H Sagor.

Table 5.1: Optimized parameters for AlGaAs, AlAs, SiGe alloy, Cu_2O, Al_2O_3 and GLS for single pole pair Lorentz model.

Materials	ε_∞	ε_s	$\delta\ (rad/sec)$	$\omega_0\ (rad/sec)$
AlGaAs	1.5376	8.2944	0.65×10^{16}	6.0×10^{13}
AlAs	2.642392	5.5635	1.885×10^{12}	6.243×10^{15}
SiGe	1.4641	12.8881	7.1×10^{10}	0.53×10^{16}
Cu_2O	1.9881	6.2001	6.1×10^{10}	0.53×10^{16}
Al_2O_3	1.001	2.057793	2.7×10^{12}	1.9678×10^{16}
GLS	2.7	5.094049	8×10^{11}	0.7×10^{16}

5.3.2 Simulating Dielectric Metal Dielectric (DMD) waveguide

We present the propagation characteristics of Surface Plasmon Polariton (SPP) in the nanoscale dielectric-metal-dielectric waveguides. The propagation losses due to absorption by constituent materials are analyzed numerically. We have investigated the structures with Silver (Ag) as metal and different dielectric materials (air, Aluminium Arsenide, Gallium Lanthanum Sulphide, Aluminium

Oxide, Silicon Germanium alloy and Cuprous Oxide) and for different wavelengths of the input signal.

The schematic diagram of the structure used for simulation is given in figure 5.3. The structure is 1000 nm in length and 1000 nm in width. The waveguide itself is 50 nm in width.

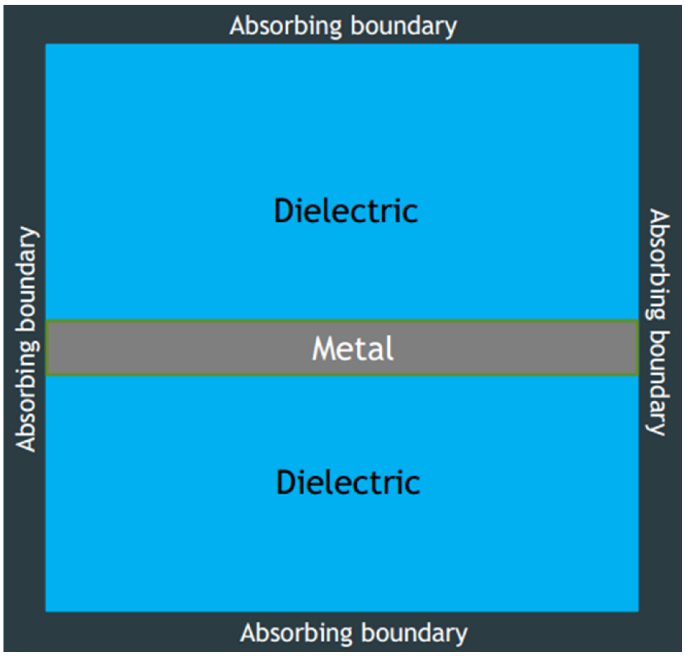

Figure 5.3: Diagram of the DMD waveguide used for simulation.

In order to model the metal we have used the six-pole Lorentz-Drude model. The frequency dependent permittivity function of Lorentz-Drude 6 (six) pole model is given by,

$$\varepsilon_r(\omega) = 1 - \frac{f_0\omega_p^2}{\omega^2 - j\Gamma_0\omega} + \sum_{i=1}^{5} \frac{f_i\omega_p^2}{\omega_i^2 + j\Gamma_i\omega - \omega^2} \qquad (5.6)$$

where, ω_p is the plasma frequency, Γ_i is the damping frequency, f_i is the oscillator strength, j is the imaginary unit and ω_i is the resonant frequency of the i^{th} pole.

At the beginning, we simulated the DMD waveguide with the input pulse given in figure 5.4 in order to generate the SPP modes. Then we pumped the mode given in figure 5.6 into the structure modulated by a Gaussian pulse having characteristic pulse width of 3 femtoseconds and different wavelengths.

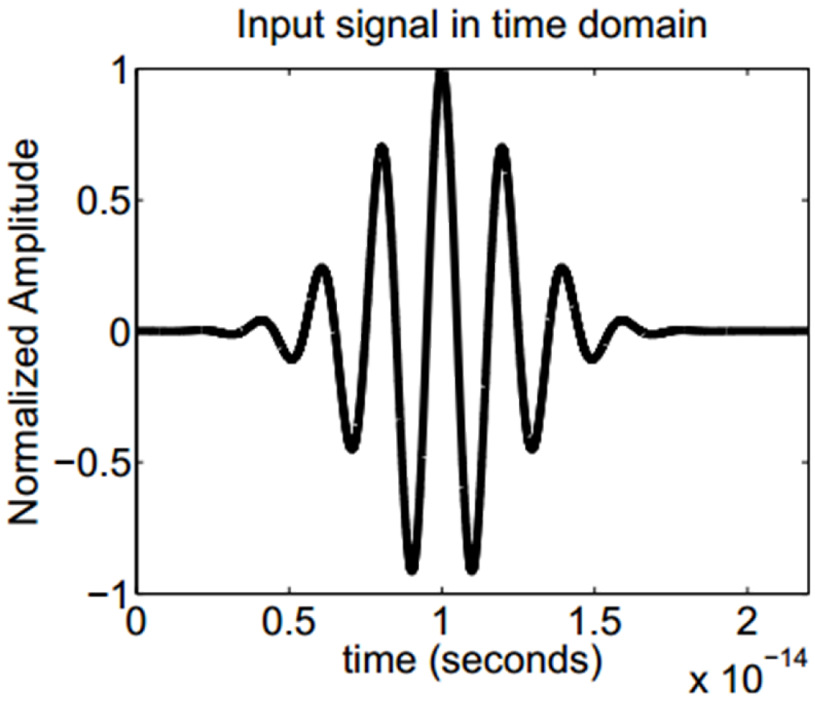

Figure 5.4: Input signal in time domain.

We simulated the system for 4000 time steps (44.784 femtoseconds). A 2D plot of surface plasmon polariton propagation in Air/Ag DMD waveguide is shown here in figure 5.5,

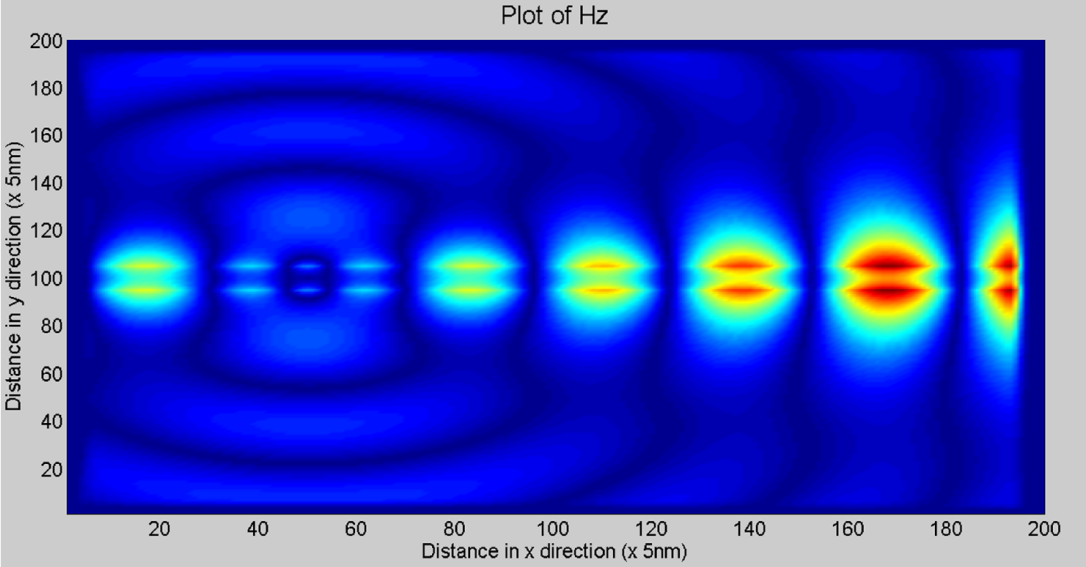

Figure 5.5: Propagation of SPP through the DMD Air/Ag waveguide after 11.196 femtoseconds

Now we generate the profile of the SPP from this simulation result. After extracting the profile we can use it to simulate any kind of Air/Ag DMD structures. The generated profile is shown in figure 5.6,

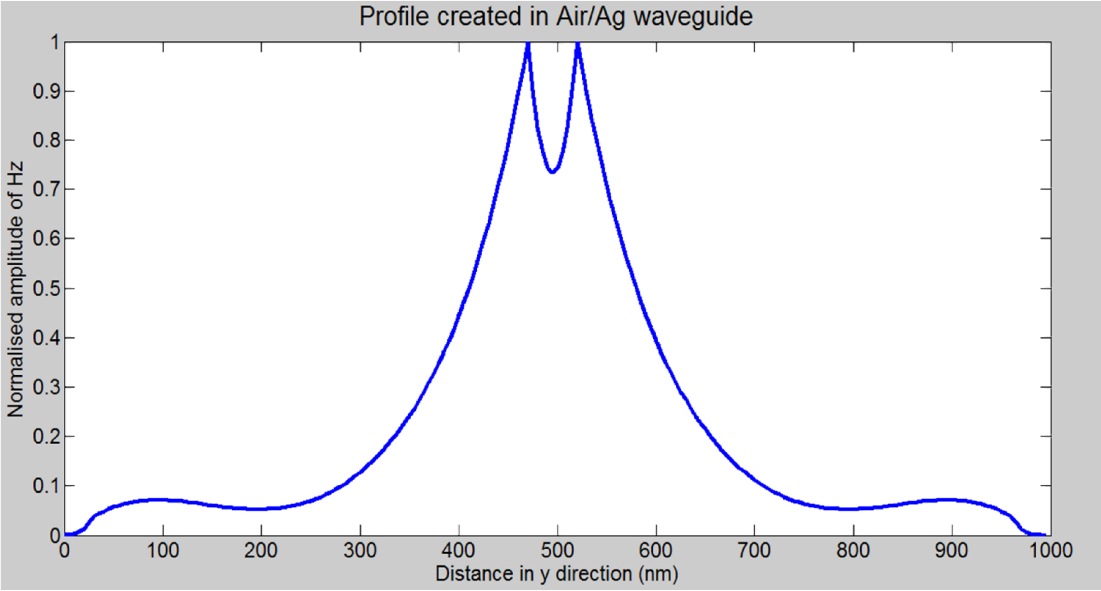

Figure 5.6: Generated SPP profile of DMD Air/Ag waveguide

5.3.3 Simulating Metal Dielectric Metal (MDM) waveguide

We present the propagation characteristics of Surface Plasmon Polariton (SPP) in the nanoscale metal-dielectric-metal waveguides. The propagation losses due to absorption by constituent materials are analyzed numerically. We have investigated the structures with Silver (Ag) as metal and different dielectric materials (air, Aluminium Arsenide, Gallium Lanthanum Sulphide, Aluminium Oxide, Silicon Germanium alloy and Cuprous Oxide) and for different wavelengths of the input signal.

The schematic diagram of the structure used for simulation is given in figure 5.7. The structure is 1000 nm in length and 1000 nm in width. The waveguide itself is 50 nm in width.

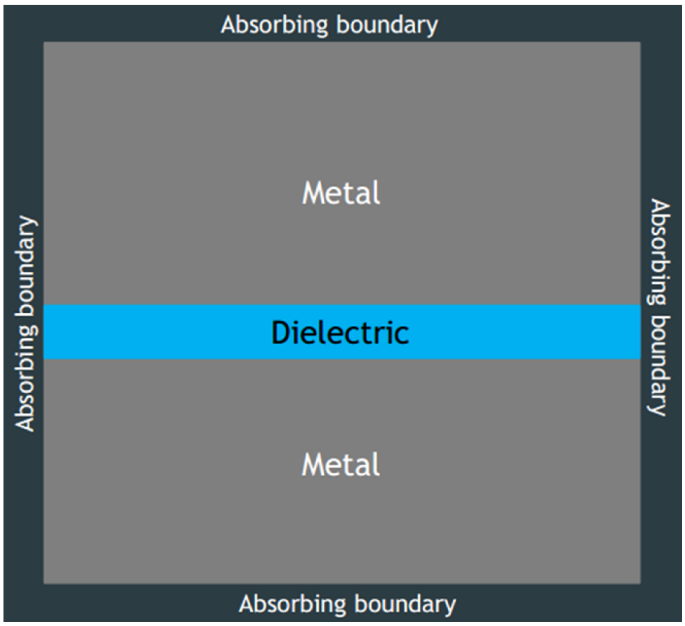

Figure 5.7: Schematic Diagram of the MDM waveguide with used for simulation.

At the beginning, we simulated the MDM waveguide with the input pulse given in figure 5.4 in order to generate the SPP modes. Then we pumped the mode given in figure 5.9 into the structure modulated by a Gaussian pulse having characteristic pulse width of 3 femtoseconds and different wavelengths.

A 2D plot of surface plasmon polariton propagation in Air/Ag MDM waveguide is shown here in figure 5.8,

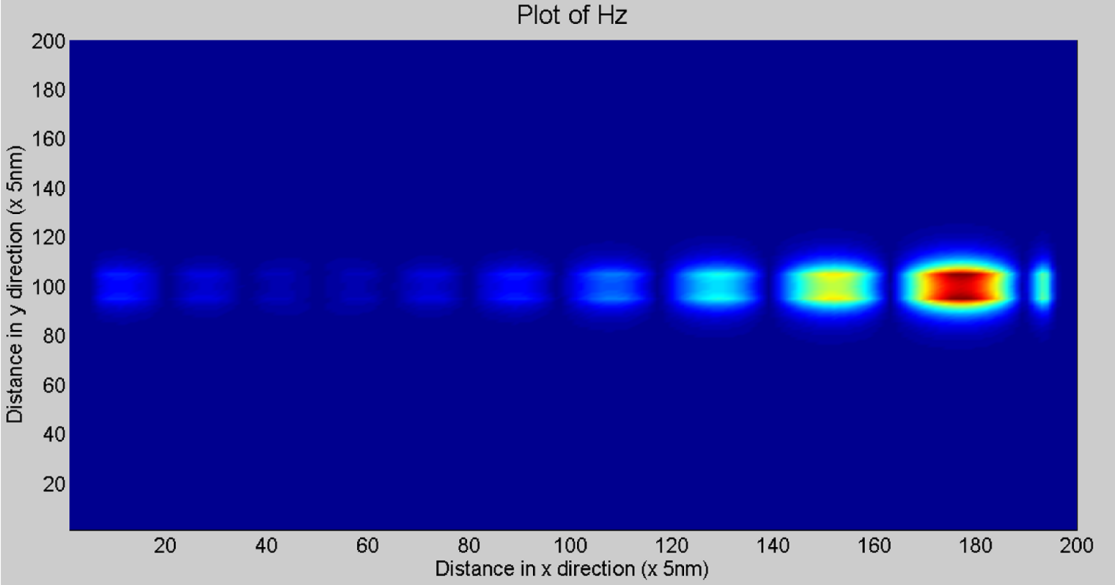

Figure 5.8: Propagation of SPP through the MDM Air/Ag waveguide after 11.196 femtoseconds

Now we generate the profile of the SPP from this simulation result. After extracting the profile we can use it to simulate any kind of Air/Ag MDM structures. The generated profile is shown in figure 5.9,

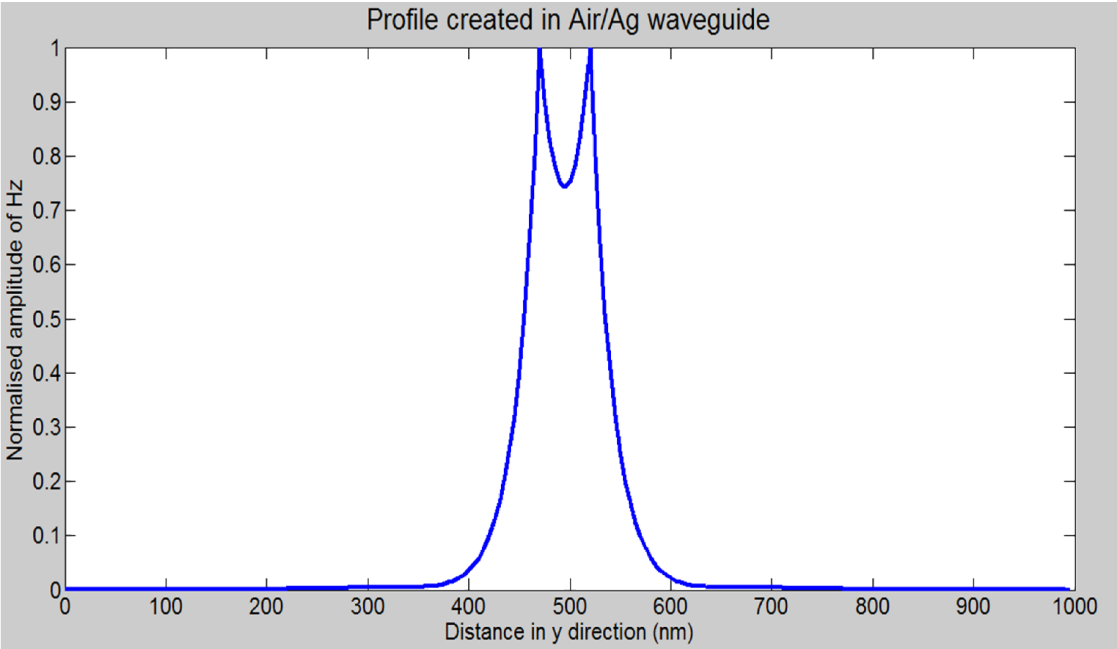

Figure 5.9: Generated SPP profile of MDM Air/Ag waveguide

5.3.4 Power transmission characteristics of simple MDM waveguides

To analyze the power transmission characteristics we've used the simple straight MDM waveguide shown in figure 5.7. We've simulated the substrate for 2000 time steps (22.392 femtoseconds) and for signals with wavelength 500 nm, 750 nm, 1000 nm and 1250 nm. We've also analyzed the waveguides using different dielectric materials.

We have used the dispersion parameters of the dielectric materials shown in the table 5.1. The parameters are based on single pole Lorentz model.

We have calculated the power and plotted it against propagation distance. The results of our analysis are shown in the following figures:

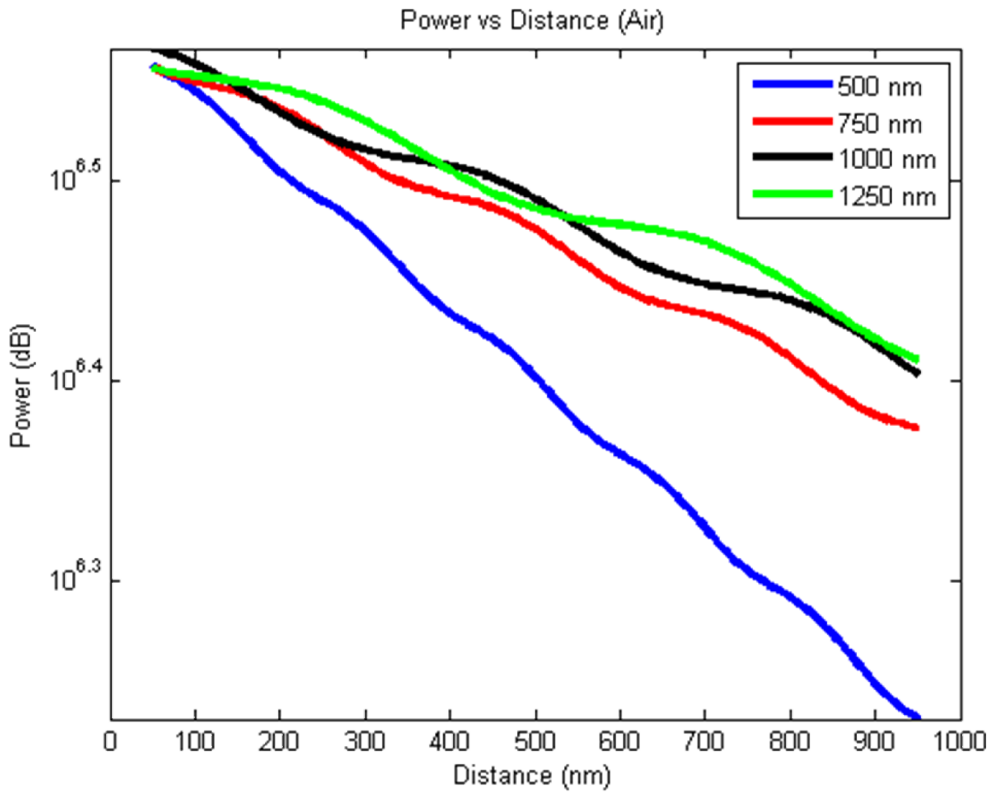

Figure 5.10: Power vs. Propagation distance graph for MDM Air/Ag waveguide

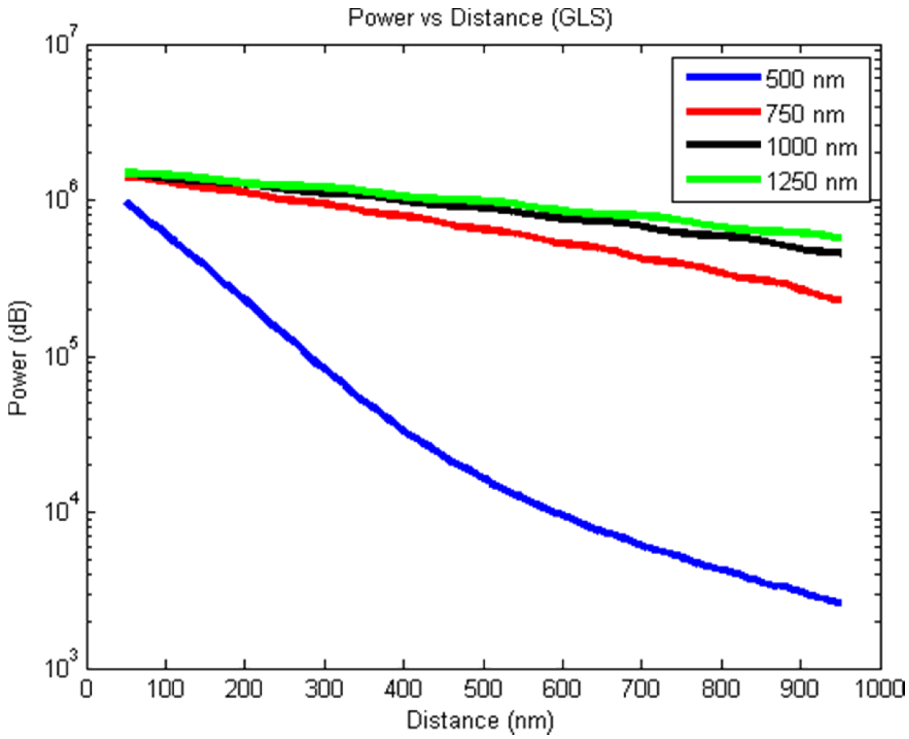

Figure 5.11: Power vs. Propagation distance graph for MDM GLS/Ag waveguide

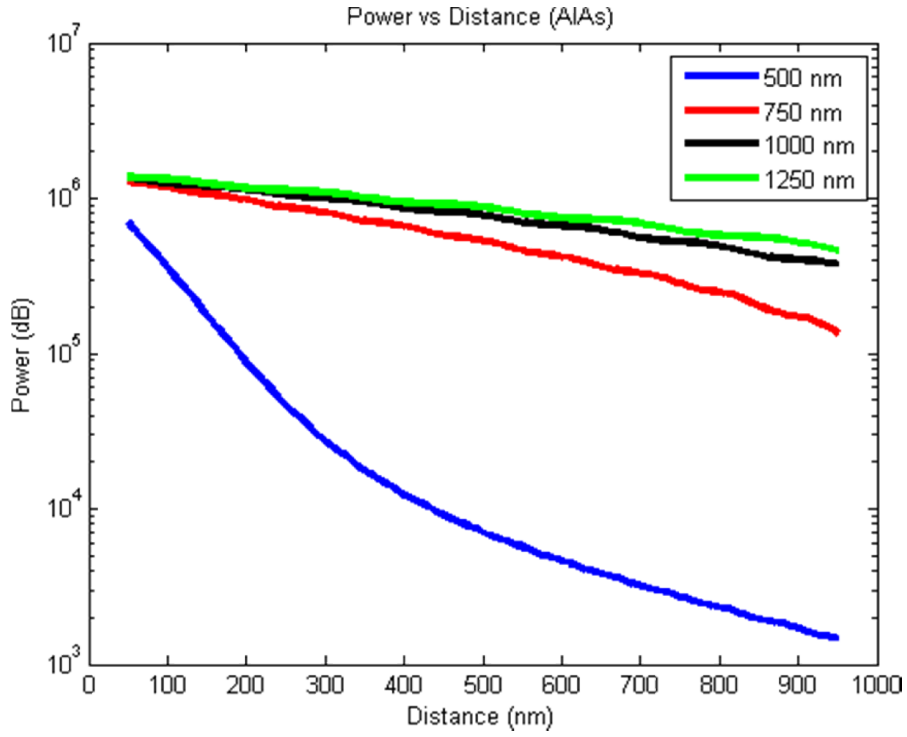

Figure 5.12: Power vs. Propagation distance graph for MDM AlAs/Ag waveguide

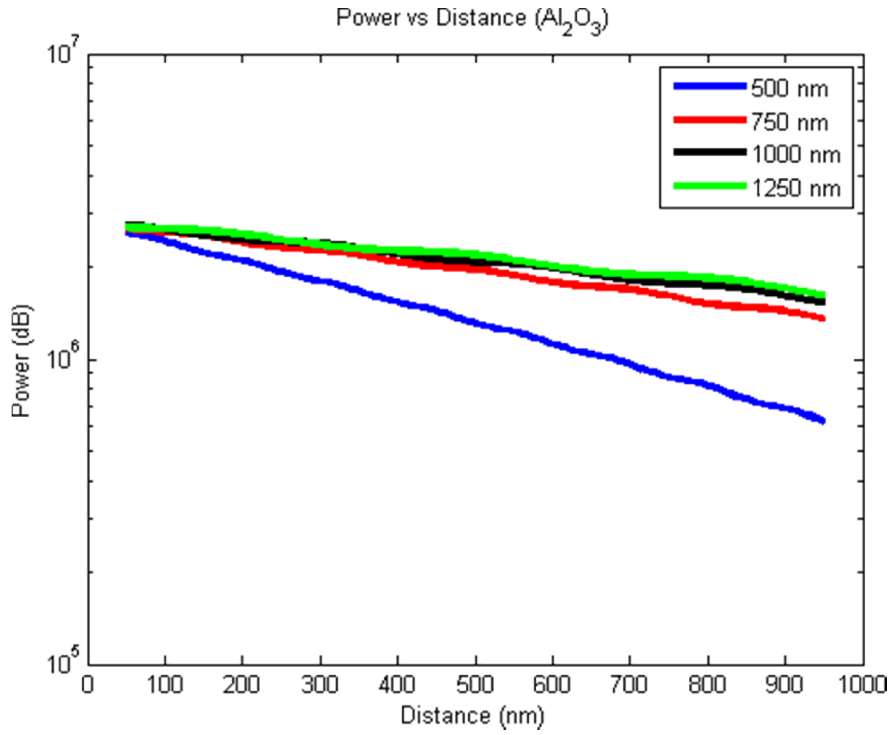

Figure 5.13: Power vs. Propagation distance graph for MDM Al_2O_3/Ag waveguide

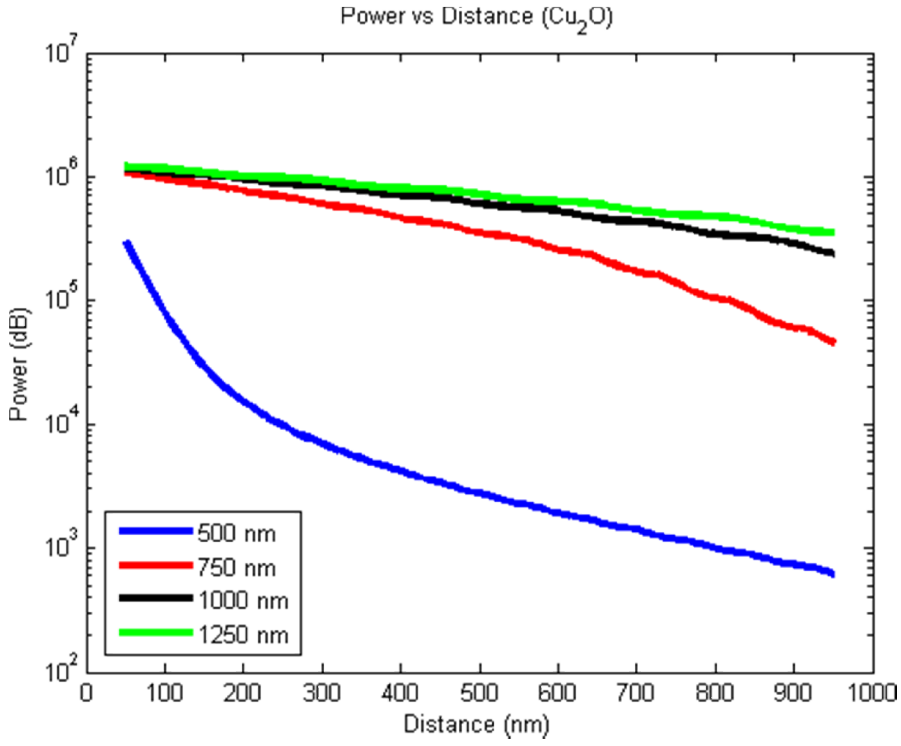

Figure 5.14: Power vs. Propagation distance graph for MDM Cu_2O/Ag waveguide

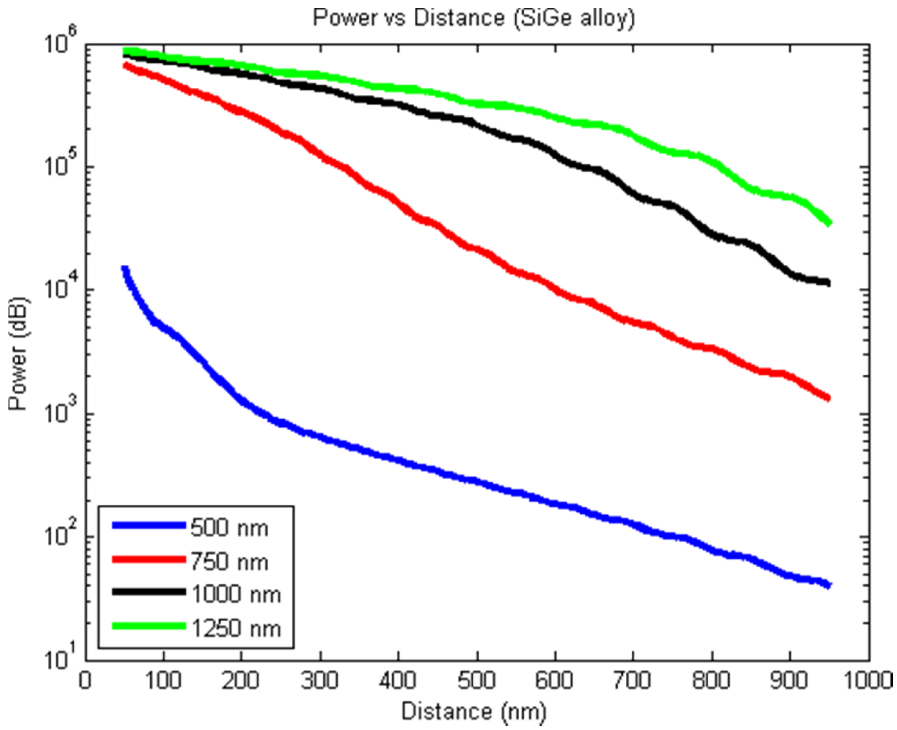

Figure 5.15: Power vs. Propagation distance graph for MDM SiGe/Ag waveguide

From our analysis we see that normally efficiency of power transmission increases if the wavelength is increased or the frequency is decreased. But there are lot of exceptions. The relationship between efficiency and wavelength is discussed in detail in the next section.

5.3.5 Efficiency of simple MDM waveguides for varying wavelengths

We've seen that the transmission efficiency depends on the wavelength of the signal. So, we've also investigated the relationship between the efficiency and the wavelength.

To do this we've used the simple MDM waveguide shown in figure 5.7. We've simulated the substrate for 2000 time steps (22.392 femtoseconds) and for signals with wavelength starting from 300 nm to 1000 nm.

Input power is calculated at 50 nm from source and output is calculated at 950 nm from source.

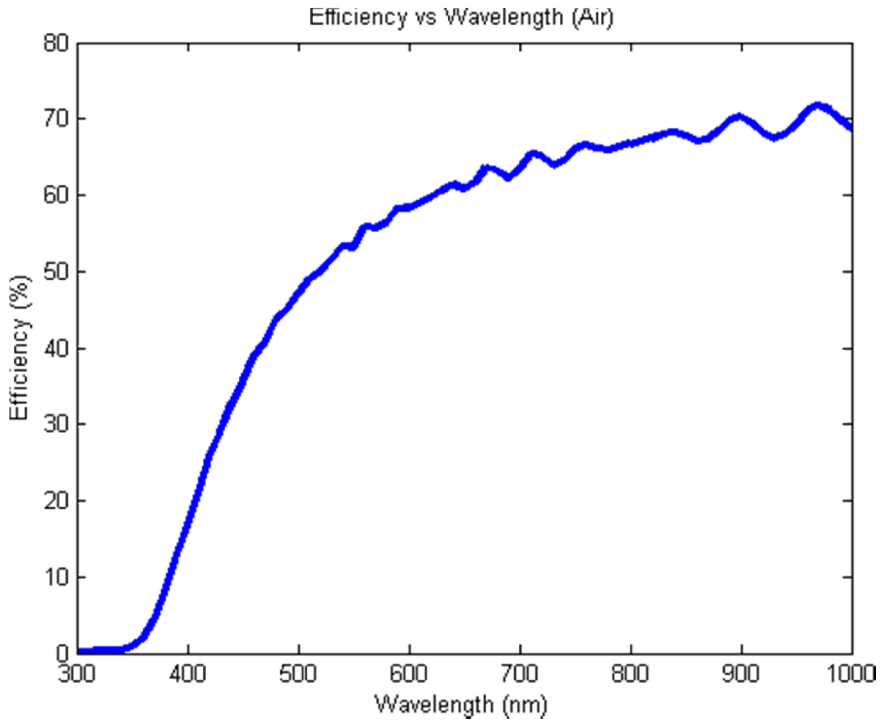

Figure 5.16: Efficiency vs. wavelength graph for MDM Air/Ag waveguide

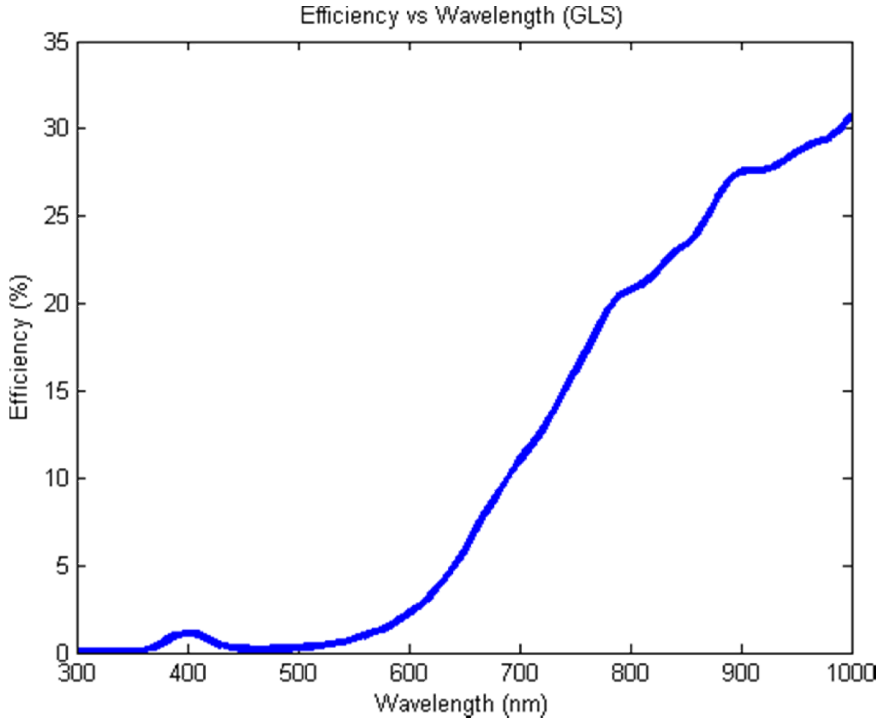

Figure 5.17: Efficiency vs. wavelength graph for MDM GLS/Ag waveguide

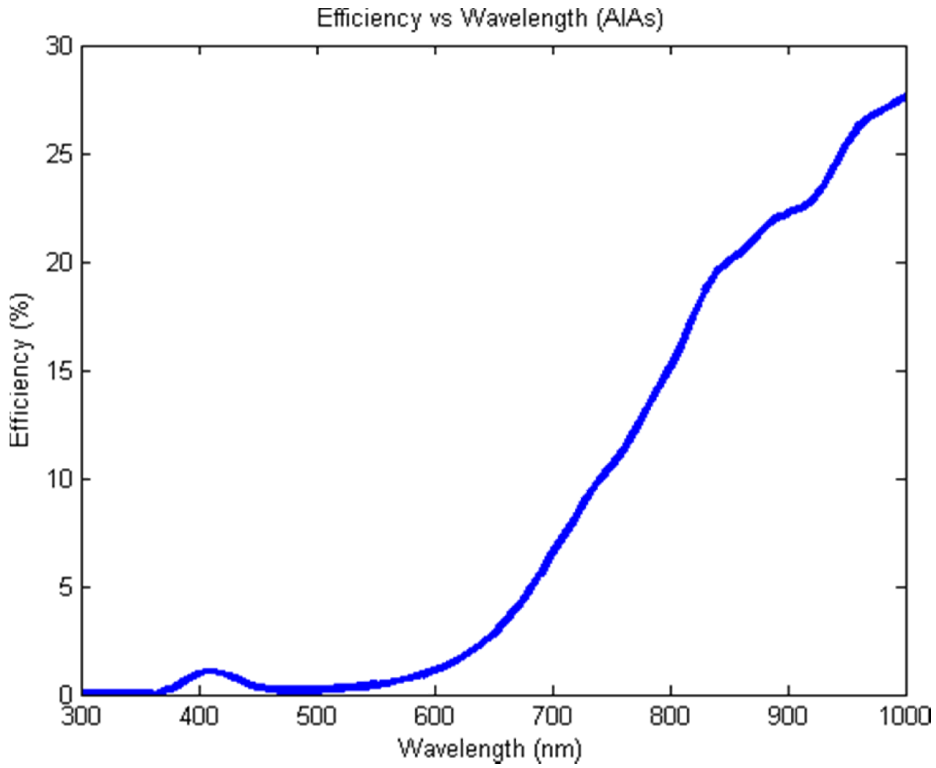

Figure 5.18: Efficiency vs. wavelength graph for MDM AlAs/Ag waveguide

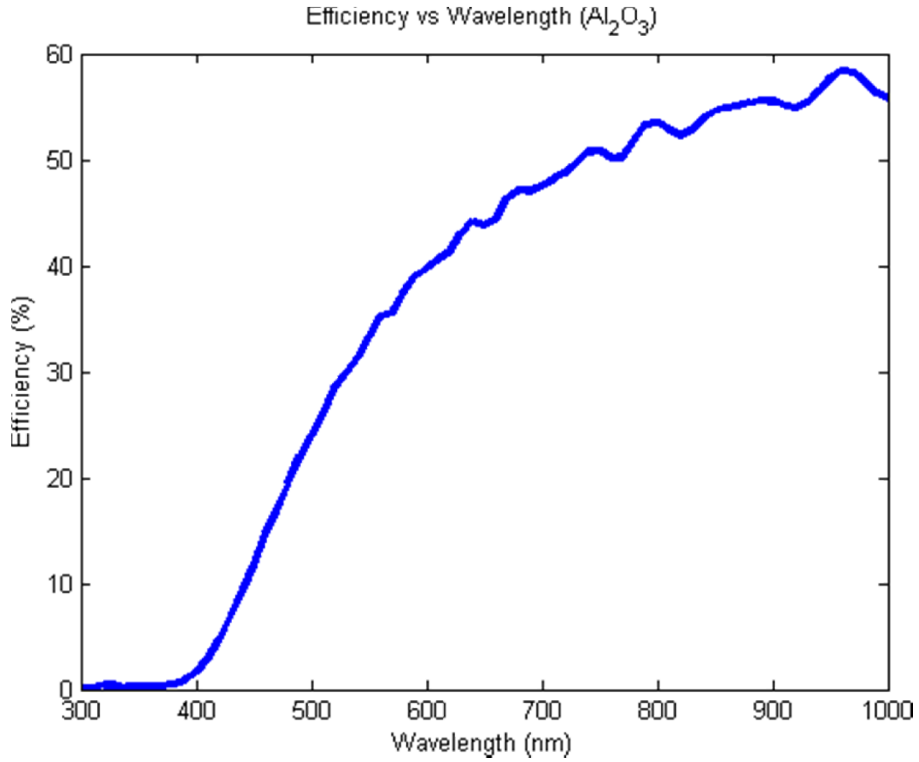

Figure 5.19: Efficiency vs. wavelength graph for MDM Al_2O_3/Ag waveguide

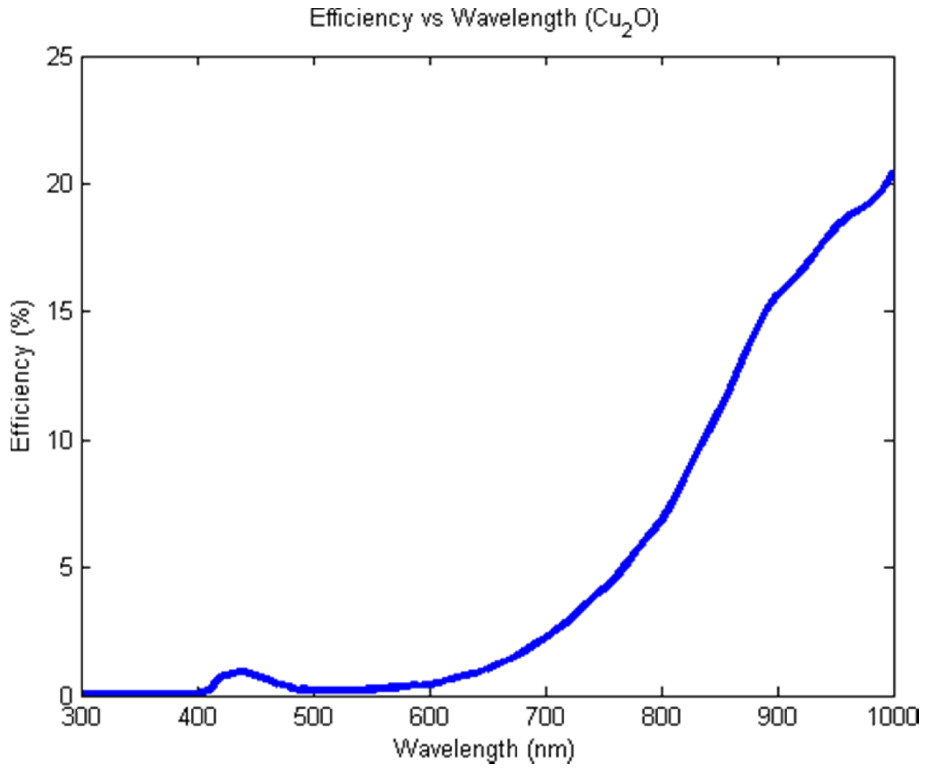

Figure 5.20: Efficiency vs. wavelength graph for MDM Cu_2O/Ag waveguide

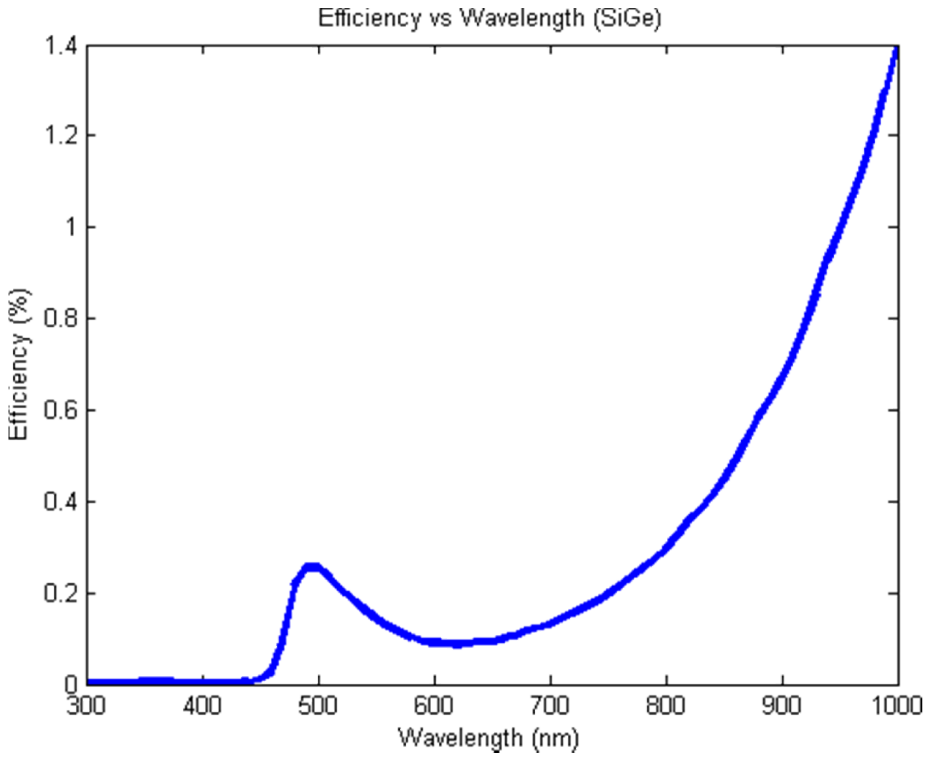

Figure 5.21: Efficiency vs. wavelength graph for MDM SiGe/Ag waveguide

We can see that the relation between transmission efficiency and wavelength is neither linear nor it can be expressed as a function. Transmission efficiency and wavelength have a complex relationship.

This relation is different for different materials. The comparison of efficiency vs. wavelength graphs for all analyzed materials is shown in figure 5.22.

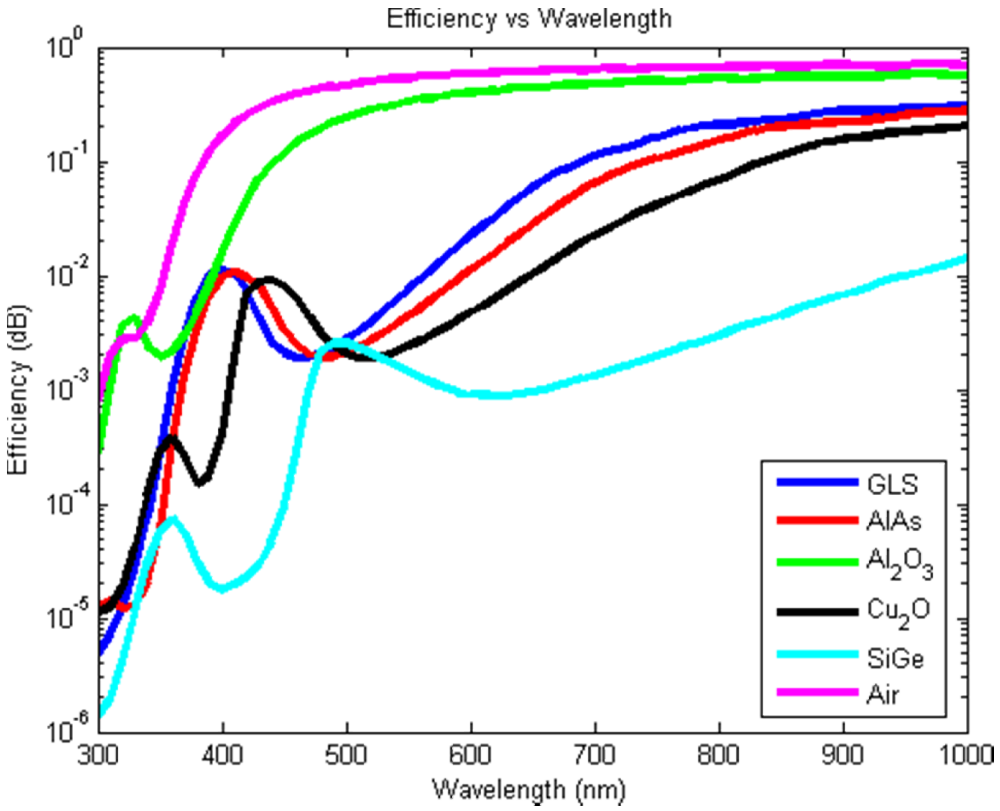

Figure 5.22: Efficiency vs. wavelength graph for different materials

So, different materials are efficient at different frequencies. From our study we are able to find the following information:

1. Air is the most efficient medium as waveguide for most of the case except for wavelength from 320 nm to 335 nm.
2. Al_2O_3 is the second most efficient material except for wavelength from 320 nm to 335 nm and from 370 nm to 395 nm. For the first case, Al_2O_3 is more efficient then air and is the most efficient material in this region.

For the second case, Al_2O_3 is less efficient than GLS and is the second most efficient material in this region.

3. GLS (Gallium Lanthanum Sulphide) is the third most efficient material for wavelength 350 nm to 370 nm, 395 nm to 390 nm and 500 nm to 1000 nm.
4. AlAs is the third most efficient material for wavelength 300 nm to 315 nm and 410 nm to 430 nm.
5. Cu_2O is the third most efficient material for wavelength 315 nm to 350 nm and 430 nm to 490 nm.
6. SiGe alloy is the third most efficient material for wavelength 490 nm to 500 nm.

5.3.6 Efficiency of MDM waveguides sharply bent at 90°

In the previous sections we've discussed our study on simple straight MDM waveguides. Now we'll talk about study on waveguides sharply bent at 90°. The dimension of the substrate is same as previous cases. The bent is located at the middle of the waveguide. The shape of the waveguide can be understood clearly from the figure 5.23.

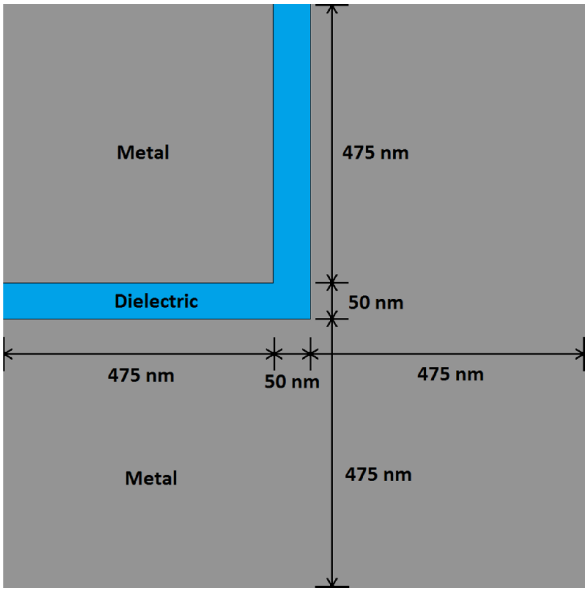

Figure 5.23: MDM waveguide with a 90° bent at the middle

We've calculated the power and compared with the previous results (for the cases with no bends).

The results are shown in the following figures:

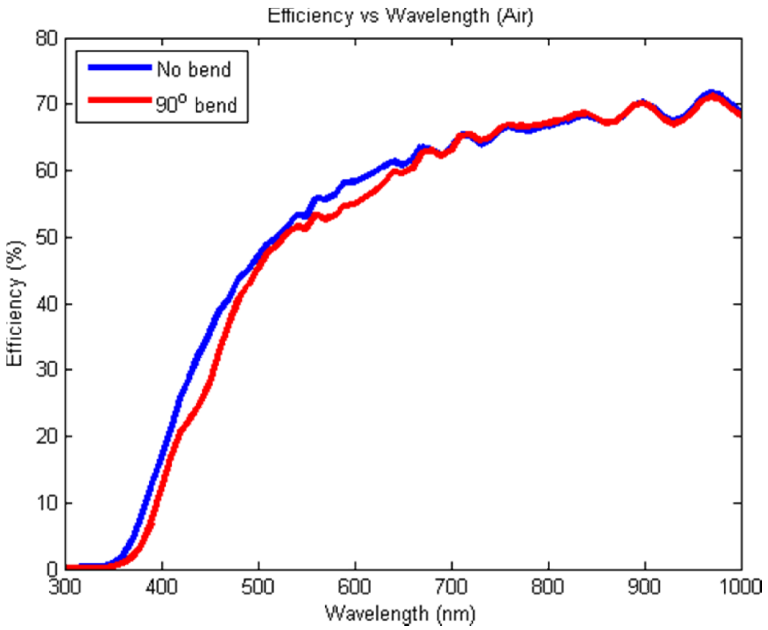

Figure 5.24: Efficiency vs. wavelength graph for no bend and 90° bend (Air/Ag)

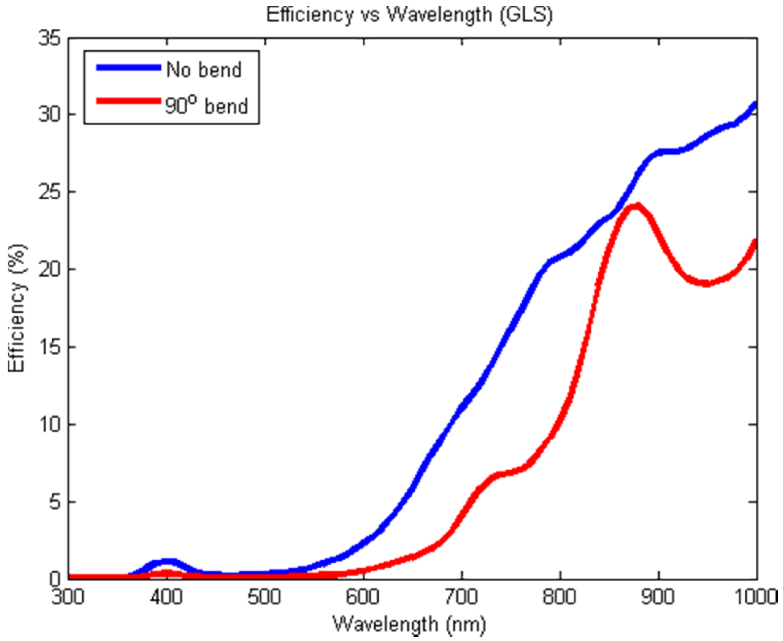

Figure 5.25: Efficiency vs. wavelength graph for no bend and 90° bend (GLS/Ag)

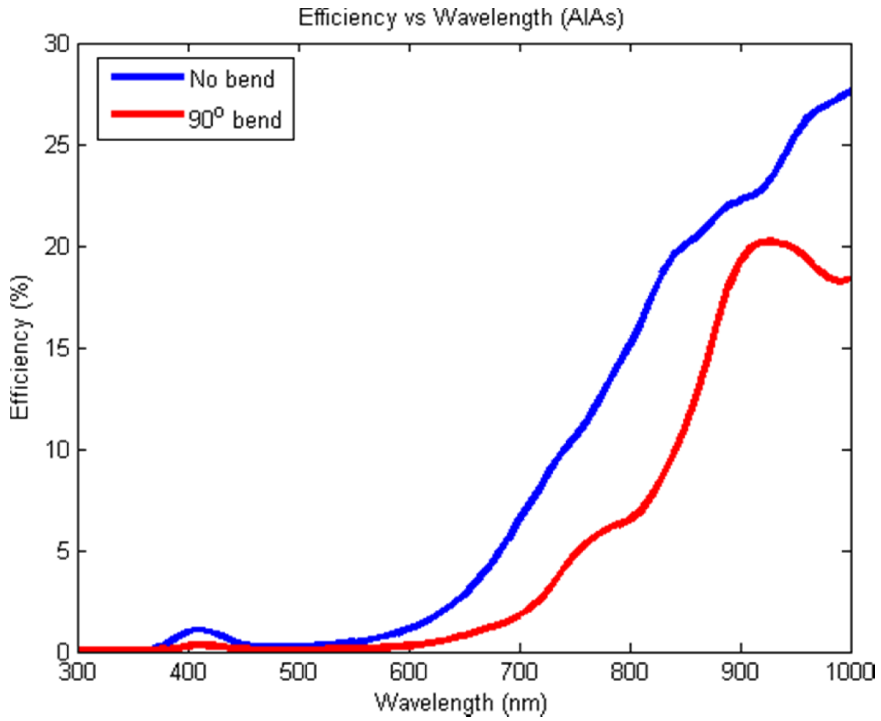

Figure 5.26: Efficiency vs. wavelength graph for no bend and 90° bend (AlAs/Ag)

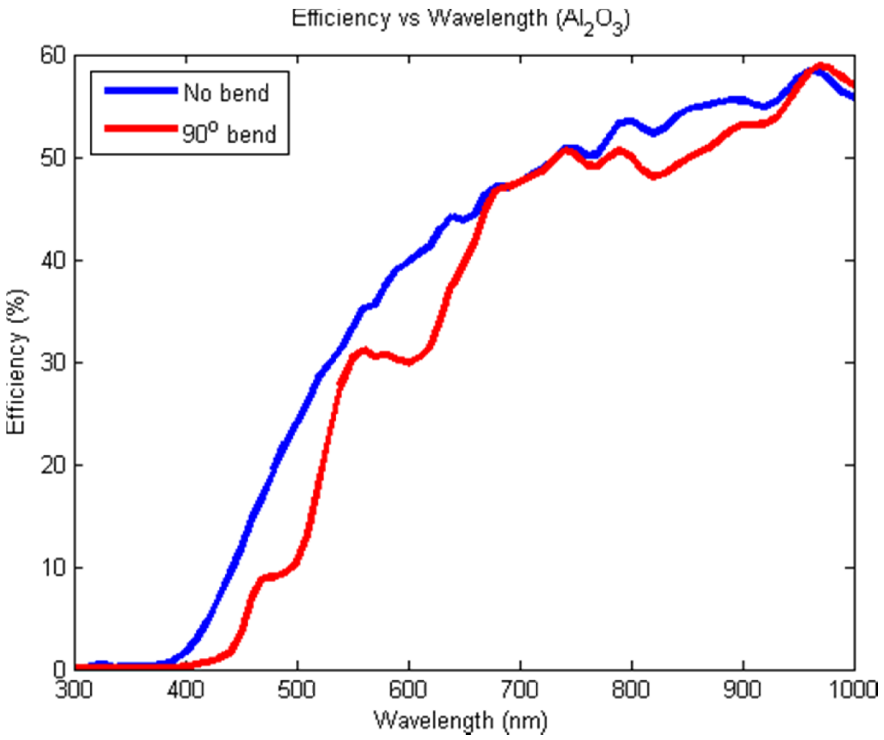

Figure 5.27: Efficiency vs. wavelength graph for no bend and 90° bend (Al_2O_3/Ag)

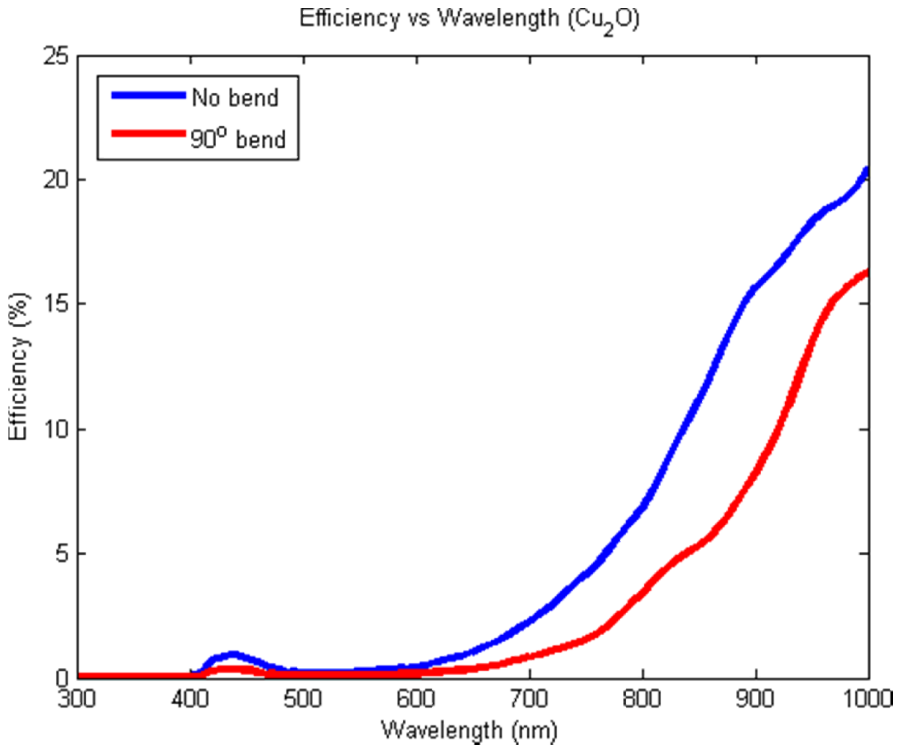

Figure 5.28: Efficiency vs. wavelength graph for no bend and 90° bend (Cu_2O/Ag)

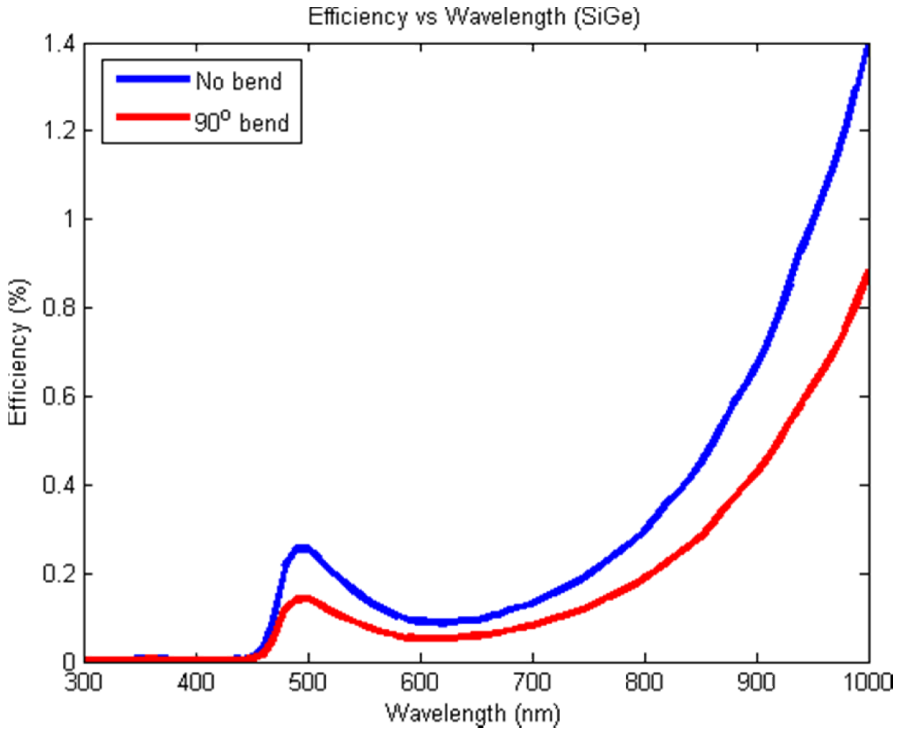

Figure 5.29: Efficiency vs. wavelength graph for no bend and 90° bend (SiGe/Ag)

5.3.7 Efficiency of MDM waveguides for circular bend

In the previous section we've investigated waveguides sharply bent at 90°. Now, we have to analyze waveguides with circular bends to find out how the efficiency varies for both cases. The dimension of the substrate is same as previous cases. The bent is located at the middle of the waveguide.

The diameter of the bend is 255 nm. The shape of the waveguide can be understood clearly from the figure 5.30.

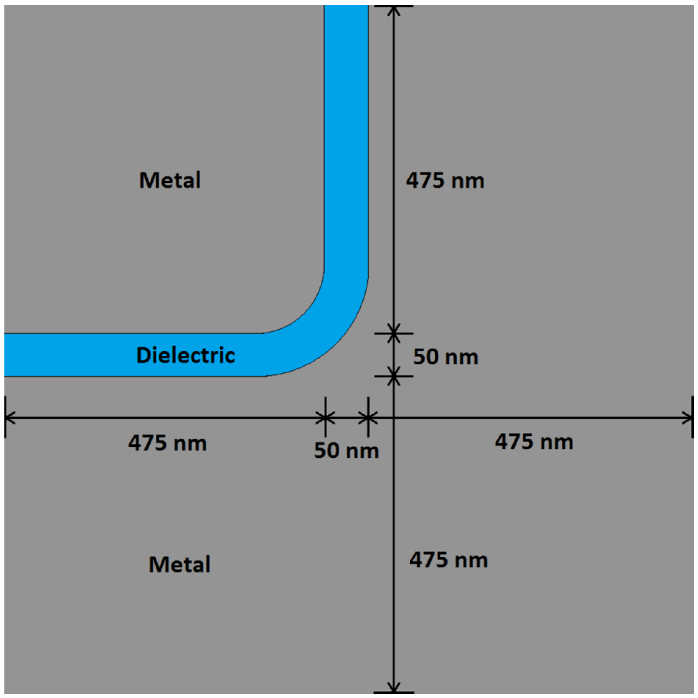

Figure 5.30: MDM waveguide with a circular bend at the middle

We've calculated the power and compared with the previous results (for the cases with sharp 90° bend).

The results are shown in the following figures:

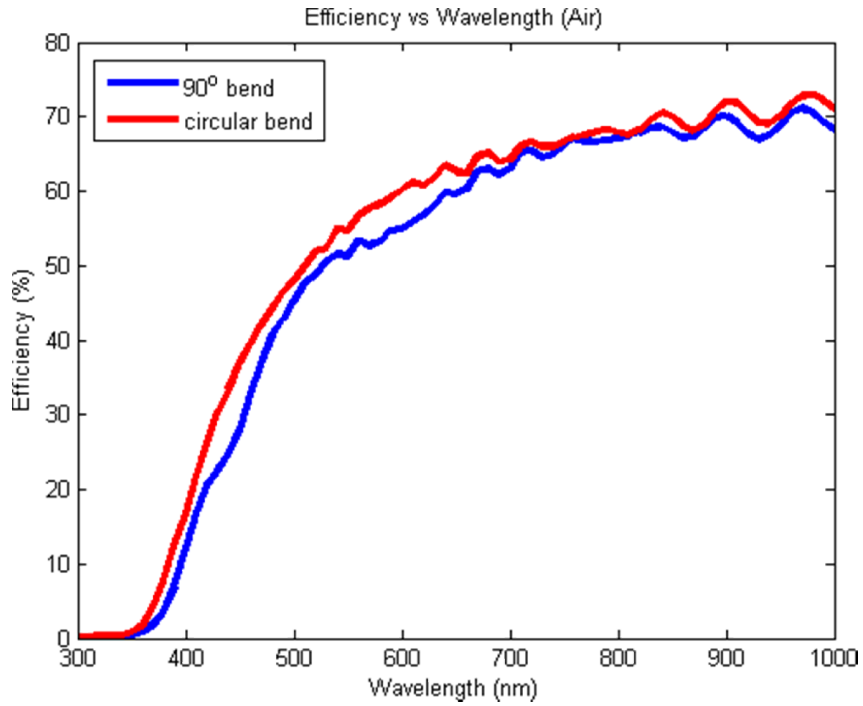

Fig 5.31: Efficiency vs. wavelength graph for circular bend and sharp bend (Air/Ag)

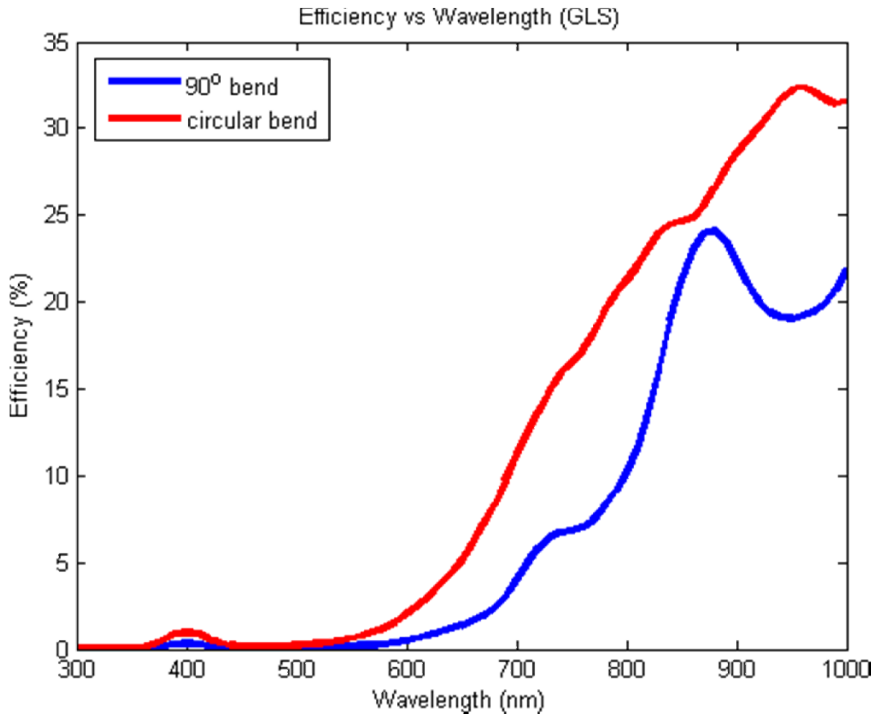

Fig 5.32: Efficiency vs. wavelength graph for circular bend and sharp bend (GLS/Ag)

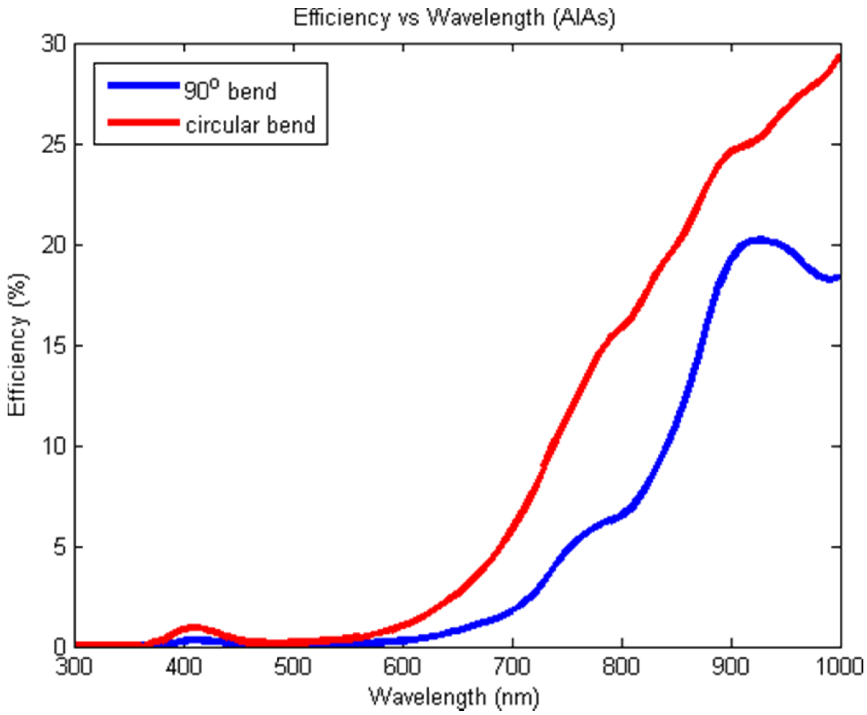

Fig 5.33: Efficiency vs. wavelength graph for circular bend and sharp bend (AlAs/Ag)

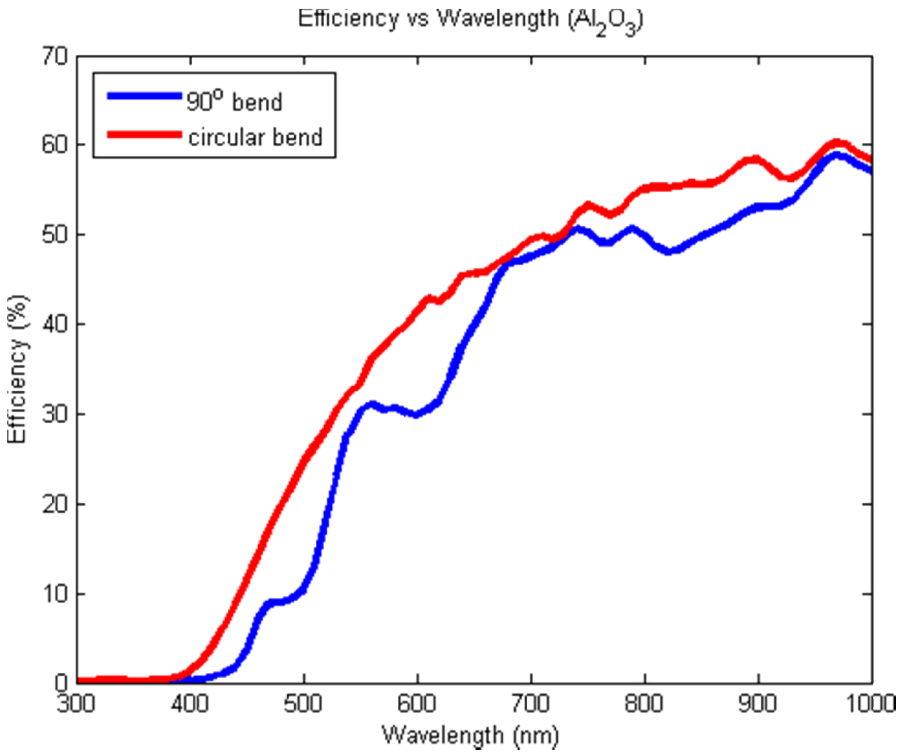

Fig 5.34: Efficiency vs. wavelength graph for circular bend and sharp bend (Al_2O_3/Ag)

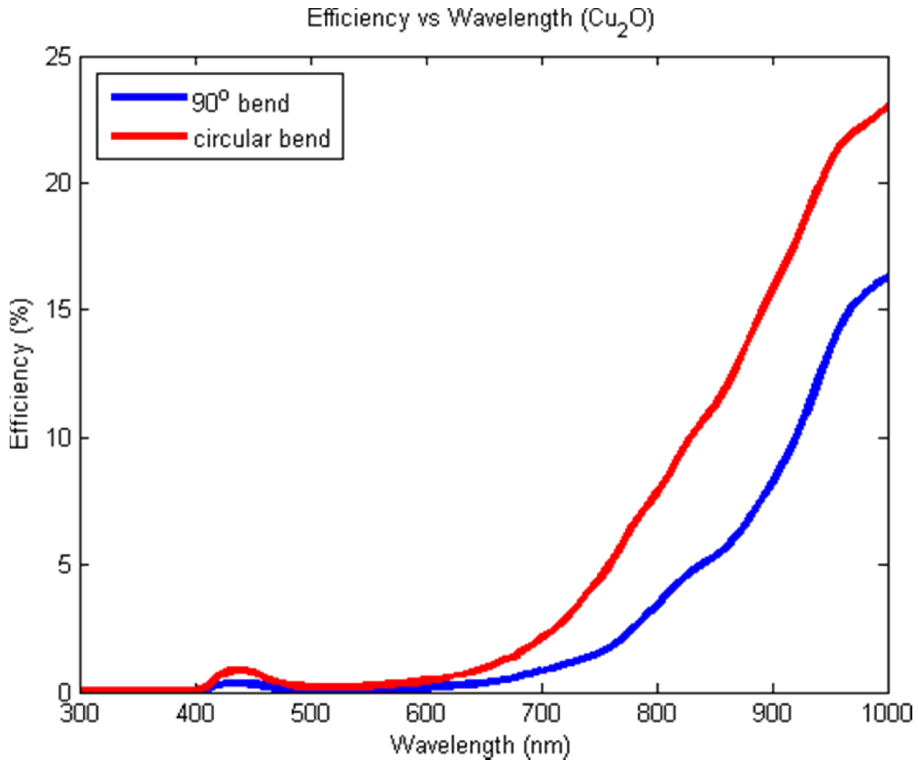

Figure 5.35: Efficiency vs. wavelength graph for circular bend and sharp bend (Cu_2O/Ag)

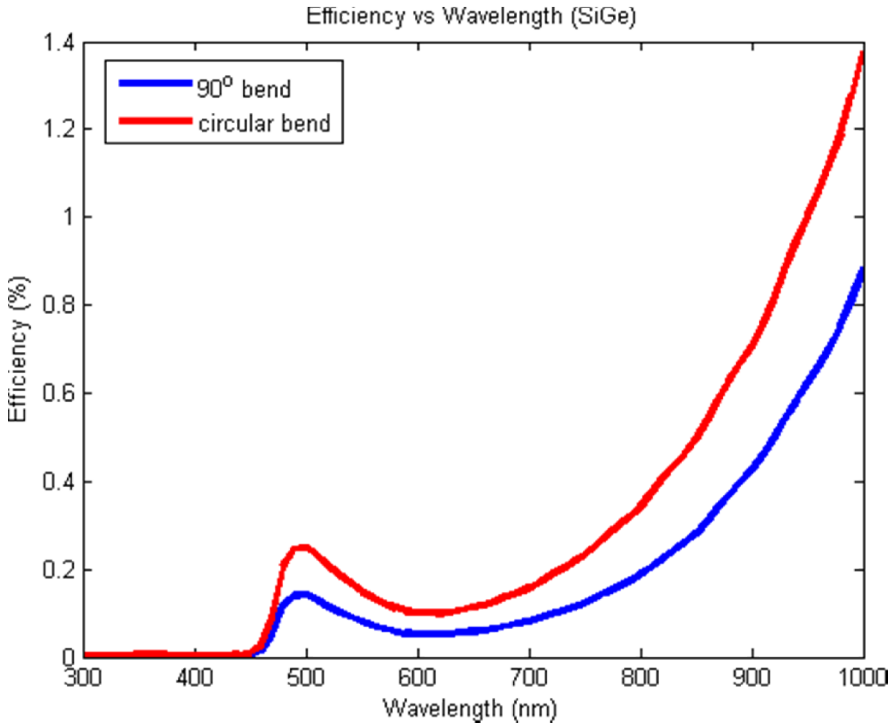

Fig 5.36: Efficiency vs. wavelength graph for circular bend and sharp bend (SiGe/Ag)

We can see that the circular bend offers much less power loss than the sharp 90° bend. Because for the sharp bend, the incident SPP perpendicularly hits the metal-dielectric surface so some portion of the SPP crosses the interface and gets absorbed. So at the output port less power is obtained. Another reason is the distance between the input and output port is less in case of the waveguide with circular bend than the waveguide with sharp 90° bend.

Chapter 6

Conclusion and Future Works

6.1 Summary and Conclusion

In this thesis, SPP propagation through different nanowaveguides has been investigated. The main contribution of this thesis is the calculation of efficiency of waveguides with different kinds of bends. Our thesis works can be summarized as follows:

- A two dimensional simulation model based on the ADE-FDTD algorithm has been developed in order to simulate different optical nanostructures. The correctness of the simulation model has been checked by simulating with the parameters given by Taflove and comparing the results with the results provided by Taflove.
- SPP propagation characteristics in dielectric-metal-dielectric (DMD) and metal-dielectric-metal (MDM) waveguide have been analyzed. Source profiles have been created for further use as source in different nanostructures.
- SPP propagation characteristics in metal-dielectric-metal (MDM) waveguides have been analyzed for different dielectric materials and for different signal wavelengths. Power vs. propagation distance graphs have been drawn for various materials and wavelengths. From these graphs it can be understood that how and at which rate the power is absorbed by the materials and what is the effect of varying wavelength on the power absorption.

- The efficiency vs. wavelength graphs have been drawn for different materials. From these graphs we understand that the efficiency and the wavelength have a complex relationship. For different materials the relationships are different. Comparing these graphs for various materials we learned that for different wavelength or frequencies different materials are efficient.
- Waveguides having a sharp 90° bend at the middle have been analyzed for several materials. The efficiency vs. wavelength graphs were drawn and were compared with that of the waveguides with no bends. It is found that because of the sharp bend the power loss has been increased which makes sense.
- Waveguides having a circular bend at the middle have also been studied. By comparing the results with the results of sharp 90° bend we are able to determine which type of bend is better. It is found that the waveguide with circular bend offers less power loss compared to that of the waveguide with sharp bend.

6.2 Future works

With the current progress of our work, we have several future goals that we want to achieve.

- We want to make a numerical simulator which will be able to simulate any types of nanostructures and devices.
- We will embed the currently known dispersive parameters of different materials to the simulator so that structures can be simulated using those materials easily.
- We will work with nonlinear materials and try to extract their modeling parameters in order to include them in our simulator.
- Easy power calculation and representation for any propagation direction will also be implemented.

- Common nanostructures like couplers, resonators, waveguides and different devices will be embedded to the simulator so that the user has to spend less effort making and designing those.
- The current numerical simulator can be extended to 3D to observe the linear dispersion of different nanostructures.
- We will try to arrange some experimental setups and implement our work practically.

Bibliography

[1] A. Al-Azzawi, *Photonics: principles and practices*: CRC Press, 2006.

[2] M. Pelton and G. W. Bryant, *Introduction to metal-nanoparticle plasmonics* vol. 5: John Wiley & Sons, 2013.

[3] S. A. Maier, "Plasmonics: Metal nanostructures for subwavelength photonic devices," *Selected Topics in Quantum Electronics, IEEE Journal of,* vol. 12, pp. 1214-1220, 2006.

[4] S. A. Maier, "Plasmonics: The promise of highly integrated optical devices," *Selected Topics in Quantum Electronics, IEEE Journal of,* vol. 12, pp. 1671-1677, 2006.

[5] W. L. Barnes*, et al.*, "Surface plasmon subwavelength optics," *Nature,* vol. 424, pp. 824-830, 2003.

[6] S. A. Maier, *Plasmonics: fundamentals and applications*: Springer Science & Business Media, 2007.

[7] D. K. Gramotnev and S. I. Bozhevolnyi, "Plasmonics beyond the diffraction limit," *Nature photonics,* vol. 4, pp. 83-91, 2010.

[8] J. P. Reithmaier, *Nanostructured materials for advanced technological applications*: Springer Science & Business Media, 2009.

[9] Z. M. Wang and A. Neogi, "Nanoscale Photonics and Optoelectronics (Lecture Notes in Nanoscale Science and Technology, 9)."

[10] A. Kriesch*, et al.*, "Functional plasmonic nanocircuits with low insertion and propagation losses," *Nano letters,* vol. 13, pp. 4539-4545, 2013.

[11] K. Catchpole and A. Polman, "Plasmonic solar cells," *Optics express,* vol. 16, pp. 21793-21800, 2008.

[12] S. Y. Chou and W. Ding, "Ultrathin, high-efficiency, broad-band, omni-acceptance, organic solar cells enhanced by plasmonic cavity with subwavelength hole array," *Optics express,* vol. 21, pp. A60-A76, 2013.

[13] S.-S. Kim*, et al.*, "Plasmon enhanced performance of organic solar cells using electrodeposited Ag nanoparticles," *Applied Physics Letters,* vol. 93, p. 073307, 2008.

[14] S. Pillai*, et al.*, "Surface plasmon enhanced silicon solar cells," *Journal of applied physics,* vol. 101, p. 093105, 2007.

[15] A. J. Haes and R. P. Van Duyne, "A nanoscale optical biosensor: sensitivity and selectivity of an approach based on the localized surface plasmon resonance spectroscopy of triangular silver nanoparticles," *Journal of the American Chemical Society,* vol. 124, pp. 10596-10604, 2002.

[16] R. J. Blaikie and D. O. Melville, "Imaging through planar silver lenses in the optical near field," *Journal of Optics A: Pure and Applied Optics,* vol. 7, p. S176, 2005.

[17] D. Melville and R. Blaikie, "Super-resolution imaging through a planar silver layer," *Optics express,* vol. 13, pp. 2127-2134, 2005.

[18] S. Kawata*, et al.*, "Plasmonics for near-field nano-imaging and superlensing," *Nature photonics,* vol. 3, pp. 388-394, 2009.

[19] J. Henzie*, et al.*, "Multiscale patterning of plasmonic metamaterials," *Nature nanotechnology,* vol. 2, pp. 549-554, 2007.

[20] A. Hosseini and Y. Massoud, "A low-loss metal-insulator-metal plasmonic bragg reflector," *Optics express,* vol. 14, pp. 11318-11323, 2006.

[21] H. Raether, *Surface plasmons on smooth surfaces*: Springer, 1988.

[22] A. Archambault*, et al.*, "Surface plasmon Fourier optics," *Physical Review B,* vol. 79, p. 195414, 2009.

[23] E. Jin and X. Xu, "Plasmonic effects in near-field optical transmission enhancement through a single bowtie-shaped aperture," *Applied Physics B,* vol. 84, pp. 3-9, 2006.
[24] J. T. Krug II*, et al.*, "Design of near-field optical probes with optimal field enhancement by finite difference time domain electromagnetic simulation," *The Journal of chemical physics,* vol. 116, pp. 10895-10901, 2002.
[25] W. H. Pernice*, et al.*, "A general framework for the finite-difference time-domain simulation of real metals," *Antennas and Propagation, IEEE Transactions on,* vol. 55, pp. 916-923, 2007.
[26] A. D. Rakić*, et al.*, "Optical properties of metallic films for vertical-cavity optoelectronic devices," *Applied optics,* vol. 37, pp. 5271-5283, 1998.
[27] M. A. Ordal*, et al.*, "Optical properties of fourteen metals in the infrared and far infrared: Al, Co, Cu, Au, Fe, Pb, Mo, Ni, Pd, Pt, Ag, Ti, V, and W," *Applied optics,* vol. 24, pp. 4493-4499, 1985.
[28] T. Holmgaard and S. I. Bozhevolnyi, "Theoretical analysis of dielectric-loaded surface plasmon-polariton waveguides," *Physical Review B,* vol. 75, p. 245405, 2007.
[29] G. Veronis and S. Fan, "Theoretical investigation of compact couplers between dielectric slab waveguides and two-dimensional metal-dielectric-metal plasmonic waveguides," *Optics express,* vol. 15, pp. 1211-1221, 2007.
[30] P. Ginzburg and M. Orenstein, "Plasmonic transmission lines: from micro to nano scale with λ/4 impedance matching," *Optics express,* vol. 15, pp. 6762-6767, 2007.
[31] R. Wahsheh*, et al.*, "Nanoplasmonic air-slot coupler: design and fabrication," in *Frontiers in optics*, 2012, p. FTh4A. 6.
[32] D. F. Kelley and R. J. Luebbers, "Piecewise linear recursive convolution for dispersive media using FDTD," *Antennas and Propagation, IEEE Transactions on,* vol. 44, pp. 792-797, 1996.
[33] R. Luebbers*, et al.*, "A frequency-dependent finite-difference time-domain formulation for dispersive materials," *Electromagnetic Compatibility, IEEE Transactions on,* vol. 32, pp. 222-227, 1990.
[34] R. J. Luebbers*, et al.*, "A frequency-dependent finite-difference time-domain formulation for transient propagation in plasma," *Antennas and Propagation, IEEE Transactions on,* vol. 39, pp. 29-34, 1991.
[35] R. J. Luebbers and F. Hunsberger, "FDTD for N th-order dispersive media," *Antennas and Propagation, IEEE Transactions on,* vol. 40, pp. 1297-1301, 1992.
[36] F. Hunsberger*, et al.*, "Finite-difference time-domain analysis of gyrotropic media. I. Magnetized plasma," *Antennas and Propagation, IEEE Transactions on,* vol. 40, pp. 1489-1495, 1992.
[37] C. Melon*, et al.*, "Frequency dependent finite-difference–time-domain [(fd) 2td] formulation applied to ferrite material," *Microwave and Optical Technology Letters,* vol. 7, pp. 577-579, 1994.
[38] A. Grande*, et al.*, "FDTD modeling of transient microwave signals in dispersive and lossy bi-isotropic media," *Microwave Theory and Techniques, IEEE Transactions on,* vol. 52, pp. 773-784, 2004.
[39] A. Akyurtlu and D. H. Werner, "BI-FDTD: A novel finite-difference time-domain formulation for modeling wave propagation in bi-isotropic media," *Antennas and Propagation, IEEE Transactions on,* vol. 52, pp. 416-425, 2004.
[40] K. S. Yee, "Numerical solution of initial boundary value problems involving Maxwell's equations in isotropic media," *IEEE Trans. Antennas Propag,* vol. 14, pp. 302-307, 1966.
[41] A. Al-Jabr and M. Alsunaidi, "A General ADE-FDTD Algorithm for the Simulation of Different Dispersive Materials," *Session 1P8,* p. 111.

[42] J.-P. Berenger, "A perfectly matched layer for the absorption of electromagnetic waves," *Journal of computational physics,* vol. 114, pp. 185-200, 1994.
[43] A. Taflove and S. C. Hagness, "Computationai Electrodynamics," *Artech house,* 2000.
[44] M. Alsunaidi and F. Al-Hajiri, "Time-domain analysis of wideband optical pulse shg in layered dispersive material," *Session 5A1 Optics and Photonics,* vol. 2, p. 795, 2009.
[45] R. H. Sagor, "Plasmon enhanced symmetric mode generation in metal-insulator-metal structure with Kerr nonlinear effect," *International Journal of Computer Applications,* vol. 50, 2012.
[46] M. G. Saber and R. H. Sagor, "Optimization of the optical properties of cuprous oxide and silicon-germanium alloy using the Lorentz and Debye models," *Electronic Materials Letters,* vol. 10, pp. 267-269, 2014.
[47] M. G. Saber and R. H. Sagor, "Design and study of nano-plasmonic couplers using aluminium arsenide and alumina," *IET Optoelectronics,* vol. 9, pp. 125-130, 2015.